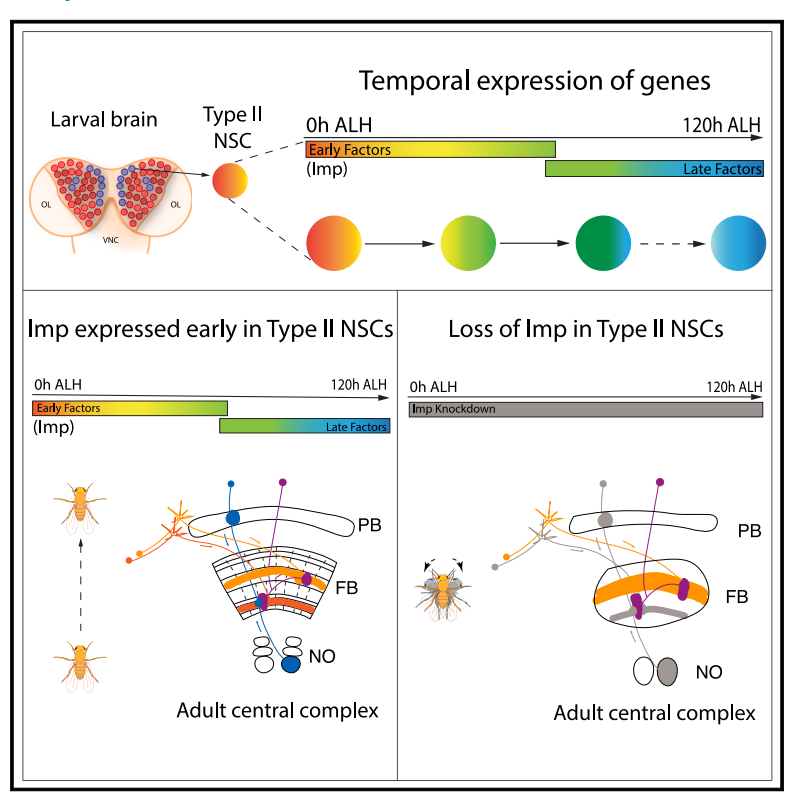
# The conserved RNA-binding protein Imp is required for the specification and function of olfactory navigation circuitry in *Drosophila*

#### **Graphical abstract**



#### **Authors**

Aisha Hamid, Hannah Gattuso, Aysu Nora Caglar, ..., Alexa Gonzalez, Katherine Nagel, Mubarak Hussain Syed

#### Correspondence

katherine.nagel@nyumc.org (K.N.), flyguy@unm.edu (M.H.S.)

#### In brief

Hamid et al. describe the lineages of olfactory navigation circuit elements in *Drosophila* and show that stem cell-specific RNA-binding protein, Imp, regulates the specification and morphology of multiple circuit elements, specifically in the central complex. Imp regulates upwind orientation in response to odor.

#### **Highlights**

- Drosophila olfactory navigation circuit components are derived from type II NSCs
- The dorsolateral type II NSC cell generates ventral FB odorencoding input neurons
- Imp governs specification and identity of the olfactory navigation circuit elements
- Loss of Imp in type II NSCs impairs upwind orientation during olfactory navigation







#### **Article**

# The conserved RNA-binding protein Imp is required for the specification and function of olfactory navigation circuitry in *Drosophila*

Aisha Hamid,<sup>1</sup> Hannah Gattuso,<sup>2</sup> Aysu Nora Caglar,<sup>1</sup> Midhula Pillai,<sup>2</sup> Theresa Steele,<sup>2</sup> Alexa Gonzalez,<sup>1</sup> Katherine Nagel,<sup>2,\*</sup> and Mubarak Hussain Syed<sup>1,3,4,\*</sup>

#### **SUMMARY**

Complex behaviors depend on the precise developmental specification of neuronal circuits, but the relationship between genetic programs for neural development, circuit structure, and behavioral output is often unclear. The central complex (CX) is a conserved sensory-motor integration center in insects, which governs many higher-order behaviors and largely derives from a small number of type II neural stem cells (NSCs). Here, we show that Imp, a conserved IGF-II mRNA-binding protein expressed in type II NSCs, plays a role in specifying essential components of CX olfactory navigation circuitry. We show the following: (1) that multiple components of olfactory navigation circuitry arise from type II NSCs. (2) Manipulating Imp expression in type II NSCs alters the number and morphology of many of these circuit elements, with the most potent effects on neurons targeting the ventral layers of the fan-shaped body (FB). (3) Imp regulates the specification of Tachykinin-expressing ventral FB input neurons. (4) Imp is required in type II NSCs for establishing proper morphology of the CX neuropil structures. (5) Loss of Imp in type II NSCs abolishes upwind orientation to attractive odor while leaving locomotion and odor-evoked regulation of movement intact. Taken together, our findings establish that a temporally expressed gene can regulate the expression of a complex behavior by developmentally regulating the specification of multiple circuit components and provides a first step toward a developmental dissection of the CX and its roles in behavior.

#### **INTRODUCTION**

Proper brain function relies on the development of intricate neural circuits that integrate and store information to generate meaningful behavior. Developmental defects can cause devastating malformations of brain circuitry in humans, with profound consequences for learning and behavior. Conversely, modifications to developmental genetic programs can underlie the evolution of more elaborate brain structures and behaviors from simpler ancestral patterns. However, the relationship between genetic programs for neural development, neural circuit structure, and behavioral capabilities is challenging to study in complex vertebrate brains.

In insects, a conserved brain structure known as the central complex (CX)<sup>5,6</sup> has been implicated in many higher-order behaviors, such as locomotion and navigation, <sup>6–21</sup> action selection, <sup>22–24</sup> steering, <sup>25,26</sup> feeding, <sup>27,28</sup> courtship, <sup>29</sup> and sleep. <sup>30–37</sup> The CX comprises several conserved structures <sup>38–41</sup> (Figure 1A), including the ellipsoid body (EB), which houses a global heading representation, <sup>15</sup> and the protocerebral bridge (PB), which broadcasts this signal to other parts of the CX. <sup>44,45</sup> The function of the fan-shaped body (FB) is more mysterious, although recent studies have

implicated this region in controlling locomotion,<sup>25</sup> computing allocentric variables, 20,21 and specifying behavioral goals. 43,46 A scaffold of columnar neurons links the different regions of the CX. Columnar inputs to the FB encode both heading information derived from the PB and optic flow or airflow information from the paired noduli (NO). 20,47 The FB also receives many tangential inputs that carry information from various parts of the dorsal brain and encode non-spatial stimuli, such as odors, 43 tastants, 28 and internal states.<sup>32</sup> Local FB neurons known as hΔ cells integrate input from columnar and tangential inputs. 43,48 Patterned stimulation of a subset of local neurons can drive reproducible navigation in an allocentric direction, implying that these neurons may encode the animal's goals. 43,46 Transmission electron microscopy (TEM) reconstruction of the hemibrain connectome<sup>49</sup> has identified 224 morphological and 262 connectivity types in the CX,48 many of which are primarily conserved in other insects such as bees.<sup>50</sup> The near-crystalline structure of the CX, along with its role in complex behaviors, make it an ideal model for investigating the relationship between neural development, circuit structure, and behavior.

Although multiple lineages give rise to the adult CX, <sup>51–53</sup> with anatomically distinct compartments, <sup>54,55</sup> the majority of adult



<sup>&</sup>lt;sup>1</sup>Department of Biology, University of New Mexico, 219 Yale Blvd NE, Albuquerque, NM 87131, USA

<sup>&</sup>lt;sup>2</sup>Neuroscience Institute, NYU Medical Center, 435 E 30th St., New York, NY 10016, USA

<sup>&</sup>lt;sup>3</sup>X (formerly Twitter): @neuroseq

<sup>&</sup>lt;sup>4</sup>Lead contact

<sup>\*</sup>Correspondence: katherine.nagel@nyumc.org (K.N.), flyguy@unm.edu (M.H.S.) https://doi.org/10.1016/j.cub.2023.12.020



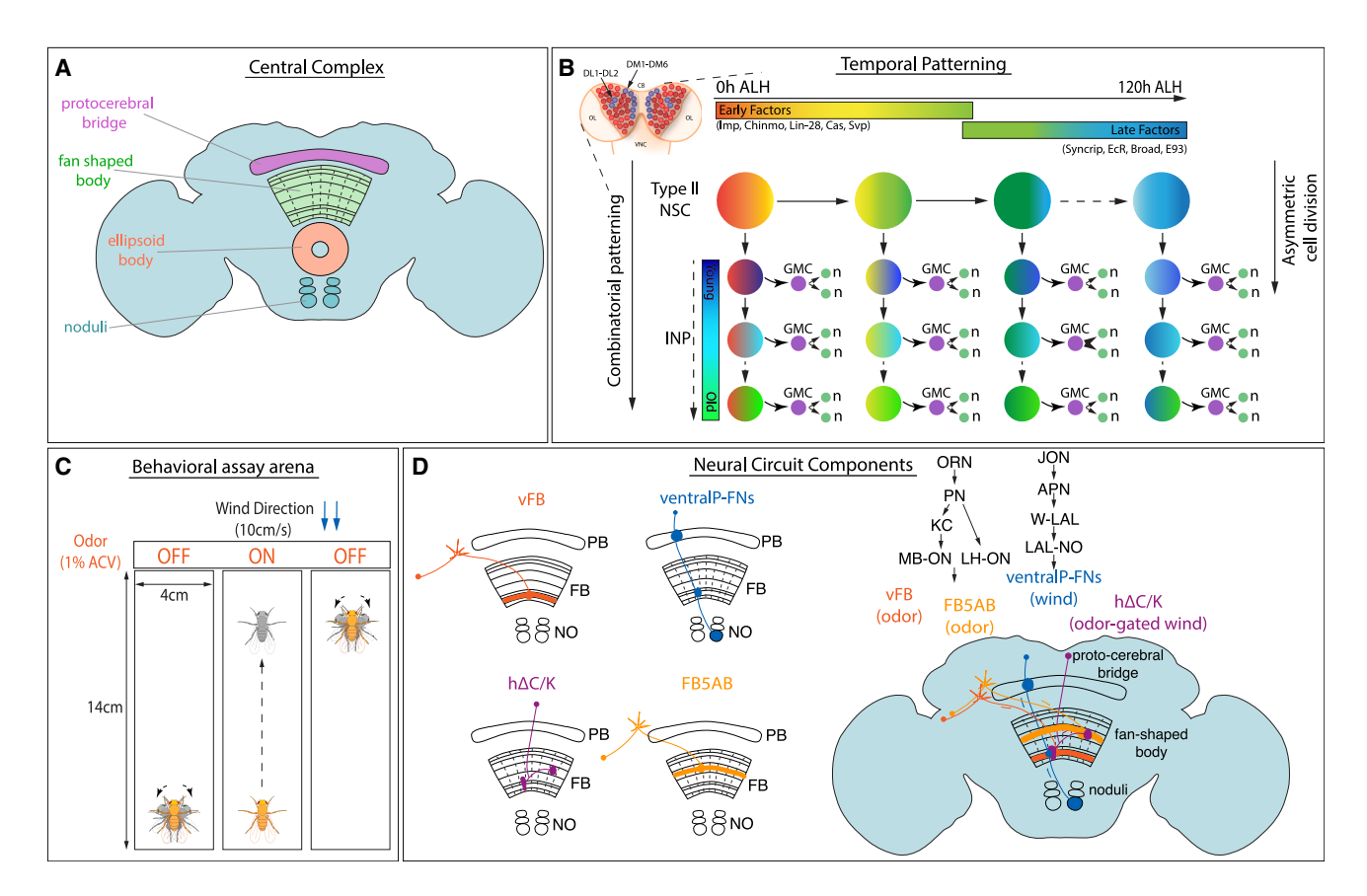


Figure 1. Overview of central complex structure and development and olfactory navigation behavior and circuitry

(A) Drosophila adult brain central complex (CX) with labeled neuropils, protocerebral bridge (magenta), fan-shaped body (green), ellipsoid body (orange), and the paired noduli (blue).

(B) Type II NSCs in the larval brain (blue, 8 per lobe: DM1–6 and DL1–2; central brain [CB], ventral nerve cord [VNC], optic lobe [OL]) divide asymmetrically to self-renew and generate an intermediate neural progenitor (INP) with each division. The INPs also divide asymmetrically to self-renew and generate a ganglion mother cell (GMC), which eventually forms two neurons and/or glia. Type II NSCs express early and late factors in a time-dependent manner starting from 0 h ALH to 120 h ALH referred to as early and late factors, respectively. In addition to temporal patterning in NSCs, INPs also express different factors in a birth-order-dependent manner along with NSC factors and give rise to a combinatorial code.

(C) Schematic of the behavioral assay arena; walking flies are observed in a rectangular chamber (14 cm × 4 cm) with constant flow of wind from one direction at 10 cm/s. Odor is provided in 10 s pulse (1% ACV) centered in a 70 s trial. Flies tend to walk upwind in the presence of odor and show search behavior triggered by odor loss. 42

(D) CX neurons involved in olfactory navigation investigated in this study. Long-field tangential neurons encode odor, and columnar ventral P-FNs encode wind. Local  $h\Delta C/K$  neurons integrate odor and wind.<sup>43</sup>

Drosophila CX neurons arise from 8 bilateral larval neural stem cells (NSCs) known as type II NSCs (based on their location: dorsomedial [DM]1-6 and dorsolateral [DL]1-2). In contrast to the more common type I NSCs, which divide to self-renew and generate a pair of differentiated neural progeny, type II NSCs divide asymmetrically to self-renew and produce an intermediate neural progenitor (INP). 56,57 INPs further divide multiple times to generate 8–12 progeny<sup>58–62</sup> (Figure 1B). The dual division pattern of type II NSCs is shared by the outer radial glia (oRG), stem cells that generate the primate and human cortex. 63-65 Intermediate progenitors have been reported in the human cortex as well. 66-68 Type II-like NSCs are also found in grasshoppers and beetles, <sup>69-72</sup> making them evolutionarily conserved progenitors that generate higher-order brain centers. The CX columnar neurons arise from four bilateral type II NSCs called DM1-4, whereas tangential neurons arise from mixed lineages, with a significant contribution from DL1.51,55

To generate diverse classes of neural types over time, type II NSCs express sets of temporally regulated transcription factors and RNA-binding proteins (RBPs).73,74 In addition, INPs have been shown to express different factors in a birth-order-dependent manner that play a role in generating neural identity. 75-78 Using RNA sequencing (RNA-seq) methods, we and others have identified about a dozen temporally expressed genes in type II NSCs. 73,74 These factors can be divided into two groups: early factors detected from 0 to 60 h after larval hatching (ALH) and late factors from 60 to 120 h ALH (Figure 1B). Early-expressed factors include the RBPs IGF-II mRNA-binding protein (Imp) and Lin-28, and the transcription factors Chinmo, Seven-up, and Castor. Late factors include the RBP Syncrip (Syp) and the transcription factors, ecdysone receptor (EcR), Broad, and ecdysone-induced protein 93 (E93).<sup>73</sup> In addition, extrinsic hormonal signaling via timely expression of the receptor EcR at  $\sim$ 60 h ALH induces an early-to-late gene transition in type II NSCs. 73 Opposing gradients

#### **Article**



Table 1. Driver lines used for each neuron class		
GAL4/LexA line	Neuron class labeled	
VT029515	vFB tangential inputs	
VT062617	hΔC/K FB local neurons	
21D07	FB5AB	
15E12/30E10	ventral P-FNs, FB column inputs	
65C03	dFB tangential inputs	
12D12	mFB tangential input	
25D01	MBONs (MBON-12)	
55C09	LH-ONs (LHAd1b2)	
38F04	descending neurons (DNp09)	

of Imp and Syp expression have previously been shown to regulate the number and morphology of neurons in the CX. <sup>74</sup> However, how these temporally expressed factors contribute to functional circuit formation and behavior is unknown.

Here, we use an innate goal-oriented behavior—olfactory navigation-and an associated neural circuit to gain insight into how developmental programs specify neural types and shape circuit structure to determine behavioral output. When a hungry fly encounters an attractive odor, it will turn and increase its velocity upwind, 42,79 a conserved behavior observed across many arthropods<sup>80</sup> (Figure 1C). In a previous study, we implicated several CX neuron types in this behavior<sup>43</sup> (Figure 1D; Table 1). The sensory cues required for this behavior-odor and wind directionare encoded by different types of FB inputs. Tangential input neurons (ventral FB [vFB], mid FB [mFB], dorsal FB [dFB], and FB5AB) innervate different layers of FB and encode odor, 43 whereas columnar input neurons (ventral P-FNs) encode wind direction.<sup>47</sup> A set of local FB neurons labeled by the line VT062617-GAL4 integrates these cues and is required for persistent upwind tracking in flies. 43 In that study, we identified this line as labeling  $h\Delta C$  neurons; however, single-cell clones revealed that this line also labels  $h\Delta K$  neurons, which project to the EB (Figures S1A-S1C). We, therefore, refer to this population as  $h\Delta C/K$ . Here, we show that all elements of this circuit are derived from type II NSCs and that Imp is required for the specification of both tangential and columnar neurons targeting the vFB. We find that different circuit elements show distinct requirements for Imp either in NSCs or post mitotically. Imp knockdown (KD) in type II NSCs shapes the gross morphology of the CX and the expression of neuropeptides within specific layers of the FB. Finally, we show that manipulating Imp expression in type II NSCs profoundly impairs olfactory navigation behavior. Collectively, our findings demonstrate a novel role of Imp in the formation and function of an olfactory navigation circuit and trace the developmental origins of distinct components of a behavioral circuit.

#### **RESULTS**

## Type II NSCs generate multiple components of an olfactory navigation circuit

The majority of the neurons populating the adult CX are derived from 16 larval type II NSCs<sup>51</sup> (schematics shown in Figure 2A).

We first asked whether previously identified elements of an olfactory navigation circuit in the CX arise from these stem cells and determined their lineage. We used an intersectional genetic strategy to express GFP in specific neuron classes in a type II-specific manner (genetic scheme shown in Figure 2B). Wor-GAL4 is expressed in all NSCs, whereas Ase-GAL80, the repressor for GAL4, is expressed only in type I NSCs, leaving GAL4 active in only type II NSCs. Flippase, now expressed only in type II NSCs, permanently flips out a stop sequence between LexAop and GFP, making type II progeny eligible to express GFP under LexA control. A neuron-class-specific LexA can then drive expression of GFP only if those neurons are derived from type II NSCs.

Using this strategy, we found that several components of the CX olfactory navigation circuitry are derived from type II NSCs. These include multiple tangential FB inputs that encode odor (vFB, mFB, and FB5AB), as well as local neurons that integrate odor and wind information (h\Delta C/K, Figures 2C-2F). We used a different genetic strategy for two additional neuron classes to determine their lineage, as we had only GAL4 and not LexA lines for these classes at the time. This strategy is based on the cell class lineage intersection (CLIn) transgenic system.<sup>81</sup> Here, multiple flip-out events mediated by Flippase, Cre, and KD recombinases restrict the clonal analysis to type II NSCs. The type-IIspecific promoter stq-14 drives the expression of the reporter A-mCherry in a lineage-specific manner, and a class-specific GAL4 drives the expression of reporter B-GFP in a type-IIdependent manner (genetic scheme shown in Figure 2G). This analysis showed that two additional components of olfactory navigation circuitry, an odor-encoding dFB tangential input and a wind-encoding columnar input (ventral P-FNs), also arise from type II NSCs (Figures 2H and 2I). Taken together, our lineage analysis shows that multiple elements of an olfactory navigation circuit in the CX arise from type II NSCs.

## Mid-aged DL type II NSCs produce odor-encoding vFB tangential input neurons

Our lineage analysis revealed that several tangential FB input neurons are derived from type II NSCs. We decided to examine the lineage and birth time of one population of vFB tangential inputs more closely. To do this, we used CLIn combined with a heat-sensitive Flippase, allowing us to determine the birth time of a specific neuronal class (complete genetic scheme shown in Figure 3A). Heat shock was given by shifting larvae to 37°C at different time points ALH (Figure 3B).

The progeny of DL1 NSCs have been earlier reported to innervate the FB in two distinct bundles, dorsal and ventral<sup>51</sup> (schematics shown in Figure 3C). Single CLIn clonal analysis revealed that most vFB neurons are derived from the DL1 NSC (number of cell bodies = 7) (Figure 3D; Video S1), and a few are derived from DMs (number of cell bodies = 2, data not shown). Next, we performed genetic birth-dating by inducing flip-out events via temporal heat shock at different developmental time points in larvae: 0, 24, 48, and 72 h ALH. This genetic birth-dating revealed that most type-II-derived vFB neurons are generated between 48 and 72 h ALH (Figures 3E–3I), an interval spanning the early-to-late gene expression switch at 60 h ALH in all type II NSCs.<sup>73</sup> The number of cell bodies counted in each sample varies; this could be due to variations in multiple flip-out events in the



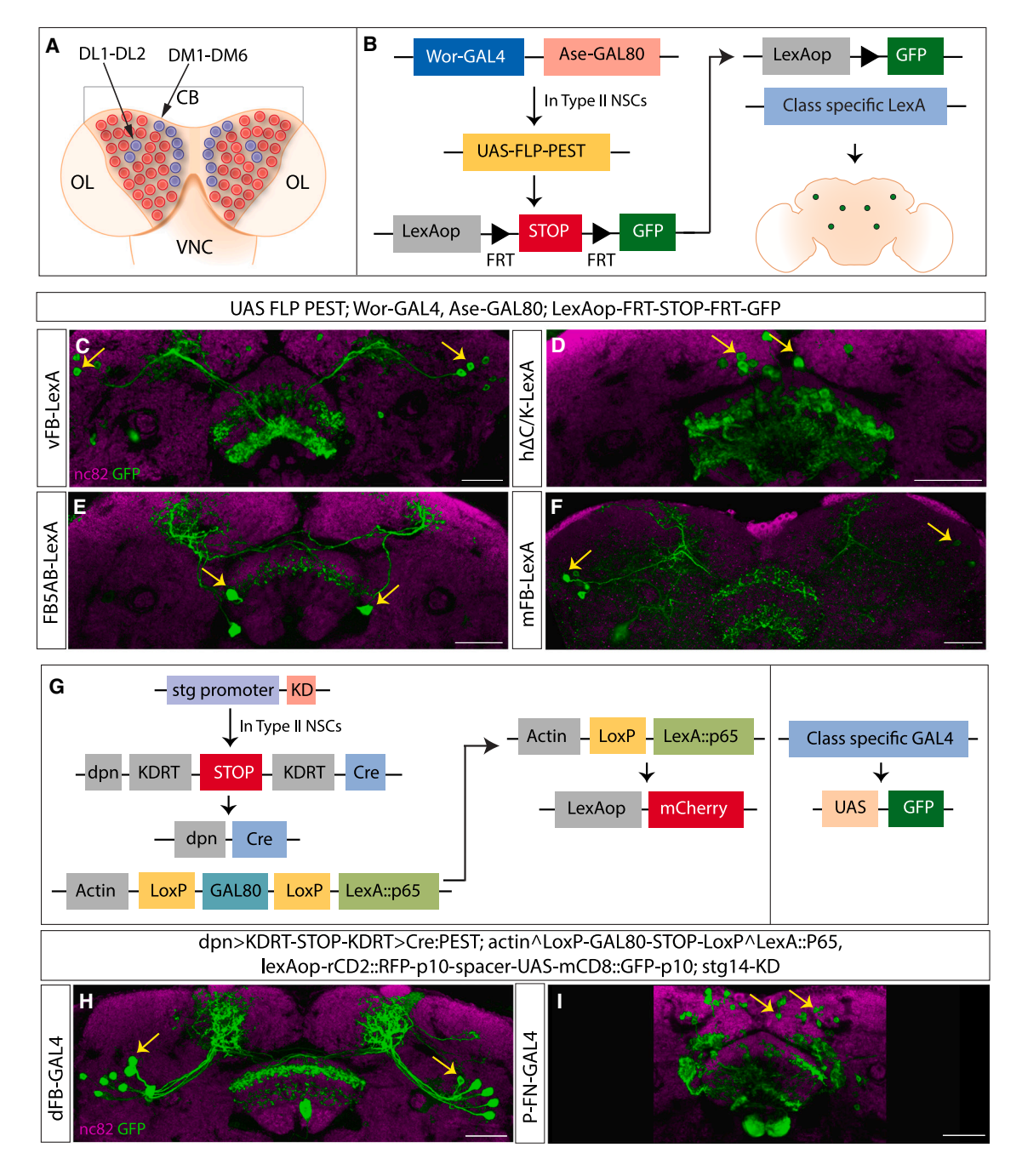


Figure 2. Lineage analysis of olfactory navigation circuit components

(A) Schematic showing 8 type II NSCs per larval brain lobe (blue) DM1–6 and DL1–2, among other NSCs (type 0 and type I) in red. Central brain (CB), ventral nerve cord (VNC), optic lobe (OL).

(B) Genetic scheme for type II lineage analysis using type-II-specific flip-out. Ase-GAL80 active in type I NSCs leaves Wor-GAL4 active only in type II NSCs. Flippase downstream of a UAS sequence is activated in a type-II-specific manner and removes the STOP sequence between two FRT sites. This causes expression of reporter GFP in class-specific manner when crossed to a class-specific LexA driver line.

(C–F) Confocal images showing neuron types expressing reporter GFP in a type-II-dependent manner.

(G) Genetic scheme for type II lineage filtering using the CLIn technique. A type-II-specific promoter fragment (stg-14) combined with KD recombinase removes a STOP sequence by a flip event and leaves Cre recombinase active in type II NSCs. Cre generates type II NSC clones positive for LexA::p65. GAL80 is active in the rest of the cells, and GAL4 expresses GFP as a reporter in class-specific manner. We did not stain for mCherry here.

(H and I) Confocal images showing neuron types expressing reporter GFP in a type-II-dependent manner. nc82 stain in magenta counterstains the brain, a stack of 2 slices was taken for visualizing the neuropil with nc82. GFP reporter is shown in green. Cell bodies are indicated by yellow arrows. The genotypes are shown at the top, and the abbreviated genotypes for neuron class are shown at the left. Scale bars correspond to 30 μm. See also Figure S1, Table 1, and Video S1.



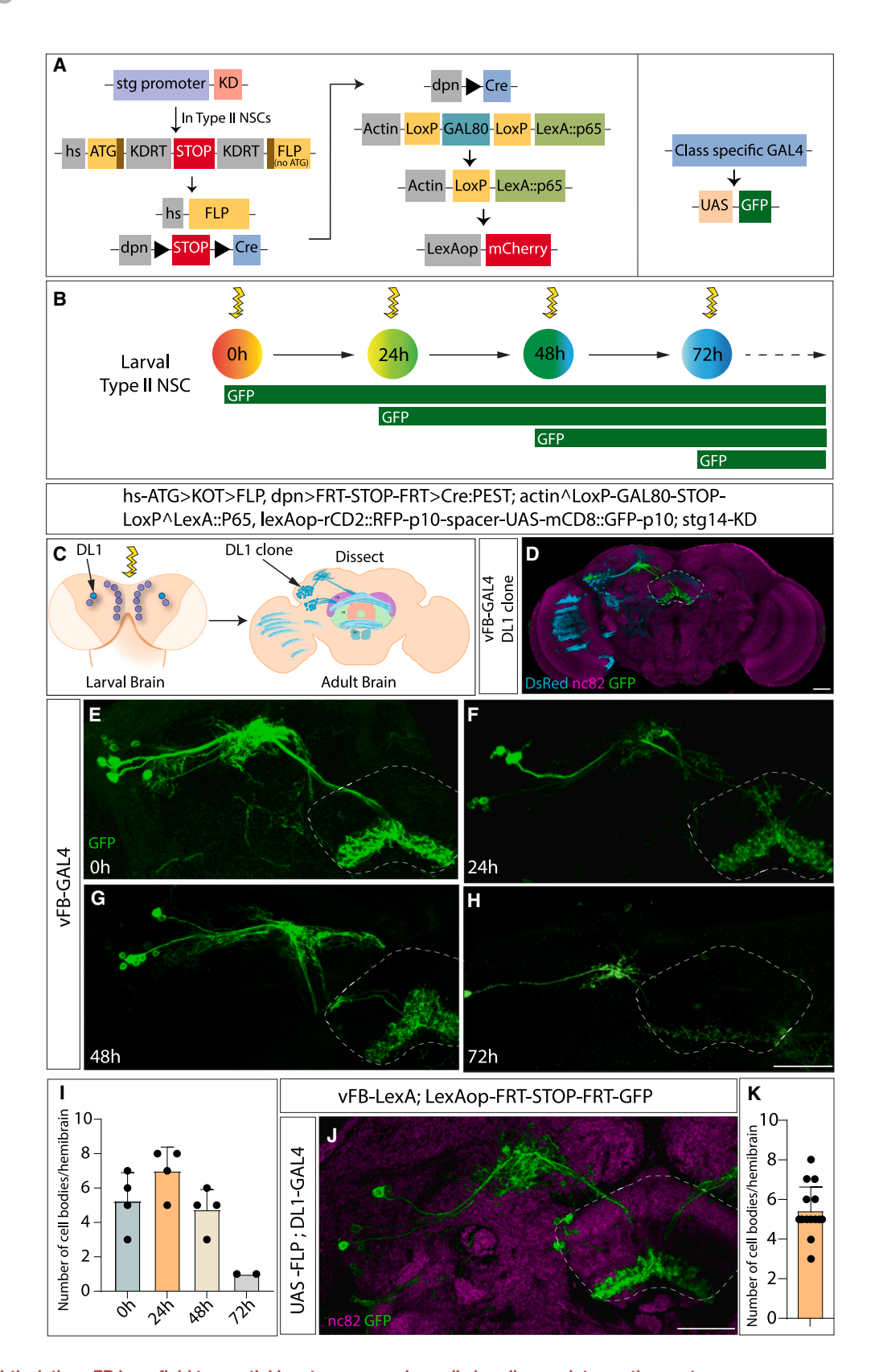


Figure 3. Birth-dating vFB long-field tangential input neurons using cell class lineage intersection system

(A) Schematics describing the genetics of the CLIn system combined with a heat shock promoter for genetic birth dating: type-II-specific stg promoter fragment combined with KD recombinase removes a STOP sequence by a flip event, and an intact Flippase is reconstituted. This, combined with a heat-sensitive



genetic technique. Combining our clonal analysis and genetic birth-dating assays, we conclude that vFB input neuron types are born from mid-aged DL1 NSCs. To confirm this result, we used an intersectional genetic strategy. From an independent screen, we identified that 17A12-GAL4 selectively labels DL1 and DL2 type II NSCs during development (Figures S1D and S1E). We used this line to express Flippase and excise an intervening STOP cassette from LexAop-FRT-STOP-FRT-GFP only in DL1 and DL2 NSCs. We combined these transgenes with VT029515-LexA to label vFB tangential input neurons. Upon expression of Flippase by 17A12-GAL4, we observed 4-8 vFB neurons labeled (n = 14 hemibrains) (Figures 3J and 3K). Variation in the number of neurons labeled might arise from variability in Flippase expression, and some vFB subtypes being derived from DM type II NSCs. These findings support our hypothesis that most vFB neuron types are born from mid-aged DL1 type II NSCs, whereas some are derived from other type II NSCs.

#### Imp regulates the specification of odor-encoding vFB tangential input neurons

Early type II NSCs express the transcription factors Chinmo, Castor, Seven-up, and the conserved RBPs, Imp and Lin-28. To test our hypothesis that an early NSC factor regulates the fate of vFB neurons, we focused on a conserved RBP, IGF-II mRNA-binding protein, Imp.82 We asked if Imp expression during development determines the number and morphology of vFB neurons. We expressed either UAS-ImpRNAi (2 copies) or UAS-Imp in type II NSCs throughout development using pointed-GAL4 that labels all type II NSCs and assayed animals at adult stages. We combined this manipulation with a LexA-based GFP reporter to examine the number and morphology of vFB neurons (VT029515-LexA). We found that Imp manipulations profoundly affected the specification of vFB neurons. In control animals, we counted about 6-7 cell bodies per hemisphere (Figures 4A, 4A', and 4H). These neurons were completely absent in type II > ImpRNAi flies (Figures 4B, 4B', and 4H). To test if Imp is sufficient for generating vFB neurons, we ectopically expressed Imp in type II NSCs, pointed-GAL4 > UAS-Imp. In these animals, Imp is now expressed in young as well as late type II NSCs.83 We observed an ~3-fold increase in the number of vFB cell bodies with Imp overexpression. These ectopic neurons formed part of the same axon bundle and similarly innervated the ventral layer of the FB (Figures 4C, 4C', and 4H). To determine whether the ectopic and endogenous vFB neurons have the same identity,

we stained for a neuropeptide Tachykinin (TK), known to be expressed in the ventral layers of the FB.84 We observed that the vFB arborization in the ventral layers of the FB colocalizes with TK immunofluorescence (Figure 4A"). Interestingly, TK expression was lost in the ventral layers upon Imp KD, suggesting an essential role of Imp in specifying neurons with TK neuropeptide identity (Figure 4B"). In contrast, Imp gain of function increased TK staining in the ventral layers, which co-localized with the innervations of the ectopic vFB neurons (Figure 4C"). To confirm that vFB neurons express TK, we drove Flippase with TK-GAL4 and used vFB-LexA > LexAop-FRT-STOP-FRT-GFP to express GFP only in vFB neurons that also express TK-GAL4. We observed 1-3 GFPpositive neurons per hemibrain (n = 6), indicating that VT029515 are, indeed, TK positive (Figures 4D-4D"). Together, these results suggest that ectopic vFB neurons are morphologically and molecularly similar to normal vFB neurons, and Imp likely regulates TK neuropeptide expression in the FB (Figures 4A"-4C").

Next, we used 17A12-GAL4 to KD Imp specifically in DL1/DL2 type II NSCs, and, as expected, we observed a significant decrease in vFB neuron number (Figures 4E, 4E', and 4I). These results suggest that Imp is required in type II NSCs to specify the majority of the DL1-derived vFB neurons. Some vFB neurons that survive could be due to weak expression of 17A12-GAL4 and/or the surviving neurons are derived from DM type II NSCs. KD of the late NSC factor Syp did not affect vFB neuron numbers (Figures S2A-S2C). Knocking down Imp using a single ImpRNAi transgene resulted in a complete loss of vFB neurons (Figures S2D-S2F), confirming the essential role of Imp in the proper development of vFB tangential input neurons.

We observed that vFB neurons continue to express low levels of Imp in adulthood (Figures 4F-4F"). This led us to ask if Imp is required post mitotically in these cells to maintain their identity. To address this question, we knocked down Imp post mitotically in these neurons using VT029515-GAL4. We observed a decrease in cell body number in Imp KD compared with control, and Imp is undetectable in the small number of surviving neurons (Figures 4G-4G" and 4J). We conclude that Imp is also required post mitotically to maintain the identity of vFB neurons.

#### Distinct roles of Imp in regulating ventral and dorsal circuit elements

We next asked whether Imp also specifies other essential neuron types of olfactory navigation circuitry. Using a similar strategy to the one described above, we knocked down or overexpressed

promoter, removes the STOP sequence and leaves Cre recombinase active in type II NSCs in a heat-shock-dependent manner. Cre, in turn, generates type II NSC clones positive for LexA::p65. GAL80 is active in the rest of the cells, and GAL4 expresses GFP as a reporter in a class-specific manner, whereas mCherry downstream of LexAop sequence is expressed as a reporter in a lineage-specific manner.

- (B) Schematics representing heat shock given at different time points (ALH, after larval hatching), yellow arrow indicates heat shock, and GFP expression window is shown in green.
- (C) Schematics showing the map of the progeny of the DL1 clone populating dorsal and ventral layers of the FB<sup>76</sup> in the adult brain.
- (D) Adult brain sample of 0 h ALH DL1 clone of CLIn crossed to VT029515 GAL4 labeling vFB neurons, nc82 counterstains the brain, a stack of 2 slices was taken for visualizing the neuropil with nc82. dsRed in cyan labels the DL1 progeny, GFP in green labels vFB neurons.
- (E-H) Adult brain samples of 0, 24, 48, and 72 h ALH clones, GFP in green labels vFB neurons.
- (I) Quantification of number of cell bodies counted per hemibrain at indicated time points (n = data points indicated on the graph).
- (J) 17A12-GAL4 flipped vFB neurons, nc82 counterstains the brain, a stack of 2 slices was taken for visualizing the neuropil with nc82. GFP in green labels vFB
- (K) Quantification of the number of cell bodies per hemibrain flipped by 17A12-GAL4. The genotypes are shown at the top, and the abbreviated genotypes for neuron class are shown at the left. Scale bars correspond to 30  $\mu m$ .



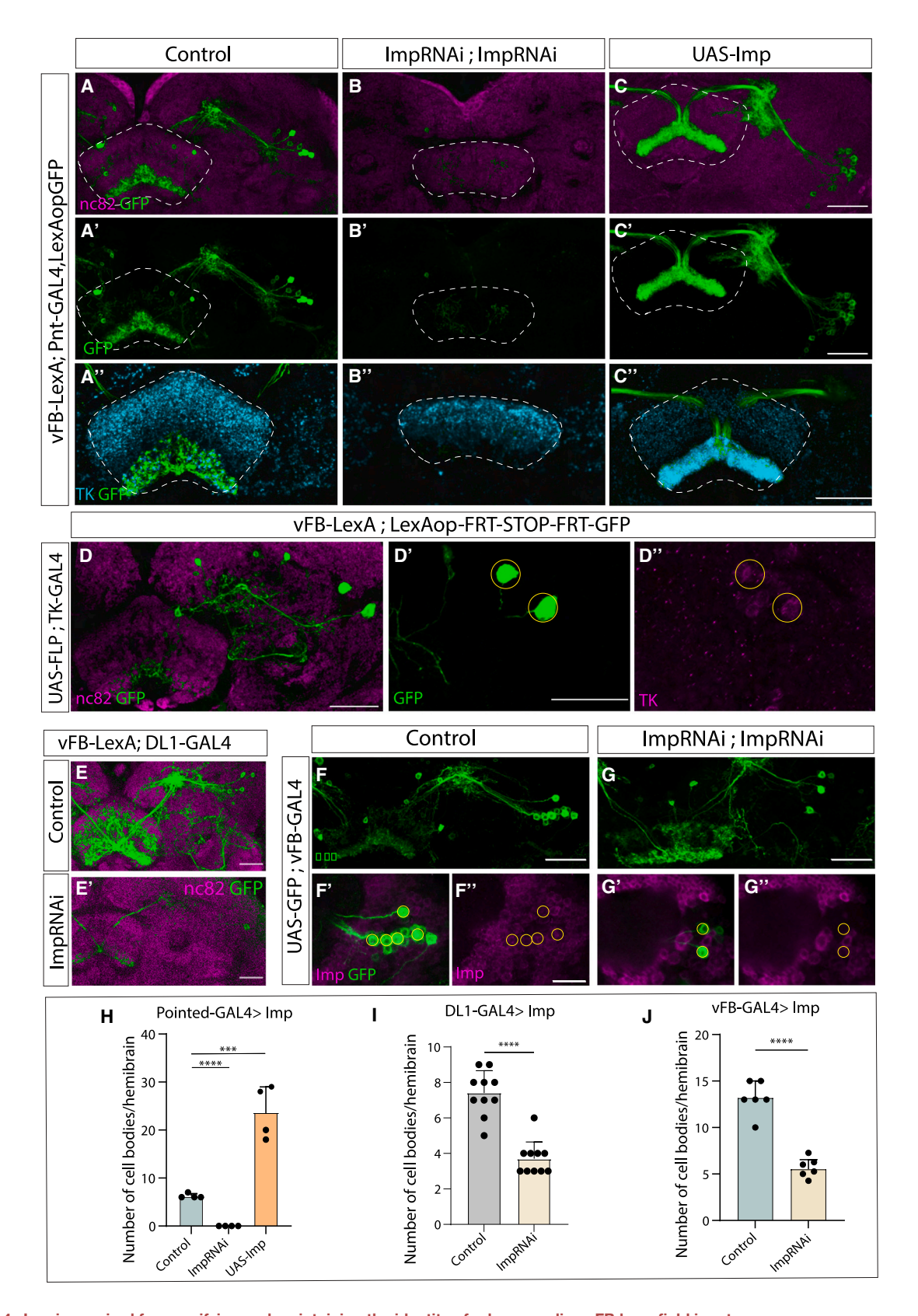


Figure 4. Imp is required for specifying and maintaining the identity of odor-encoding vFB long-field input neurons
(A–C') Effects of type-II-specific knockdown (pointed-GAL4 > ImpRNAi; ImpRNAi) or overexpression (pointed-GAL4 > UAS-Imp) of Imp on vFB neurons. vFB neurons labeled by reporter GFP in control (A), Imp knockdown (B), and Imp overexpression (C), nc82 counterstains the brain, and GFP is shown in green.



Imp during development using pointed-GAL4, a broad driver for type II NSCs, and assayed effects on each circuit element using LexA drivers and a GFP reporter in adult brains. Interestingly, we found that Imp KD in type II NSCs caused a loss of wind-sensitive columnar neurons known as ventral P-FNs (here labeled by 30E10-LexA). However, unlike vFB neurons, the number of cell bodies did not change upon Imp overexpression (Figures 5A-5C).

Because both dFB and vFB tangential input neurons respond to odor, 43 next, we wanted to know whether Imp regulates the fate of both dorsal and ventral tangential inputs. We first focused on dFB odor input neurons, which are 6-8 in number per hemibrain and project strongly to the dorsal layers and weakly to the ventral layers of the FB. We found that both Imp KD and overexpression decreased the number of tangential inputs labeled by 65C03-LexA (Figures 5D-5F). In Imp KD flies, we observed only a single projection layer. Moving to the FB5AB input neurons, we found that 21D07-LexA labels 4-6 neurons projecting to dFB per brain. We observed 2-4 cell bodies in Imp KD flies. This could be a decrease in dFB odor input neurons or loss of another subpopulation labeled by this LexA line. In Imp KD flies, the neurites of these neurons had severely impaired morphology. Imp overexpression did not alter the number of FB5AB tangential inputs, and the morphology was unaffected as well (Figures 5G-5I). The number of local hΔC/K neurons labeled by VT062617-LexA did not change upon Imp KD or overexpression (Figures 5J-5L). However, the morphology of  $h\Delta C/K$  neurons was altered in Imp KD. We observed that Imp KD caused axonal projections of  $h\Delta C/K$  to span multiple FB layers, and the division of dendrites and axons into ventral and dorsal layers was lost (Figure 5K). Together, these data suggest that Imp expression manipulations during development have the most potent effects on neurons innervating the ventral layers of the FB, including both tangential inputs (vFB) and columnar inputs (ventral P-FNs). Manipulating Imp expression had distinct effects on each neuron type, suggesting that Imp plays multiple roles and acts via multiple mechanisms to regulate cell fate and morphology. These defects suggest that neurons still present in Imp loss of function may have altered connectivity.

#### Imp regulates CX neuropil morphology and neuropeptide distribution

Our previous results show that Imp loss of function influences the morphology of the neurite projections for many of the elements within a CX olfactory navigation circuit. To test if the adult CX is more broadly altered by Imp KD in type II NSCs, we compared neuropil (nc82) stains in KD and control flies. We found that Imp

KD results in severely defective CX morphology. The PB is fragmented, the EB is only partially formed, the NO is almost entirely absent, and the FB is smaller, with no clear demarcation of layers (Figures 5Q-5T'; Videos S2 and S3). This phenotype is consistent in all pointed-GAL4 > ImpRNAi flies in Figures 4 and 5 (n = 22). The FB phenotype is reminiscent of cortical layer deformations observed in Imp1 knockout mice.85 KD of Imp in DL1/ DL2 type II NSC only using 17A12-GAL4 does not alter CX morphology and architecture (Figure S3).

Next, we wanted to examine the role of Imp in more broadly defining the neuropeptide distribution of FB layers. Previously, we described the expression pattern of the neuropeptide TK in the CX (Figure 4). We then examined the expression of short neuropeptide F (sNPF), which is reported to be strongly expressed in vFB layers 1-2 and dFB layers 6-7.84 In Imp KD flies, sNPF appears to be reduced in the dorsal layers (Figures 5U and 5U'). Together, these results suggest that both the overall morphology of distinct neuropils and neuropeptide distribution of the CX are dependent on Imp expression in type II NSCs during development.

#### Imp is required in type II NSCs for upwind orientation during olfactory navigation behavior

Given the profound effects of type-II-specific Imp expression on olfactory navigation circuitry, we sought to understand the impact of Imp on adult olfactory navigation behavior. We used pointed-GAL4 to KD Imp in type II NSCs, as in our anatomical experiments, using two copies of ImpRNAi. We then measured behavioral responses to a 10-s pulse of attractive odor (1% apple cider vinegar) using a previously described wind tunnel paradigm.42

Knocking down Imp in all type II NSCs significantly impaired olfactory navigation behavior. In control flies (pointed-GAL4 > mCherryRNAi), odor evoked an increase in upwind velocity, an increase in groundspeed, and a decrease in angular velocity, whereas odor loss evoked an increase in turning (Figures 6A and 6C), as observed previously. 42 Odor also increased the probability of movement, and this effect outlasted the stimulus by tens of seconds. In Imp KD flies (Figures 6B and 6C), upwind velocity, ground speed, and angular velocity responses to odor were dramatically reduced. However, an odor-evoked increase in the probability of movement was still observed, arguing that the olfactory system is still functional and can influence motor behavior. To better understand these behavioral deficits, we decomposed upwind velocity during odor into two components: upwind orientation and ground speed. Upwind orientation was strikingly decreased in Imp KD

(A"-C") vFB neuron arbors shown by GFP expression in green, neuropeptide TK staining shown in cyan colocalizing with GFP for control (A"), Imp knockdown, expression observed in dorsal layers of FB (B") and Imp overexpression, TK expressed in thick bundle colocalizing with GFP expression (C").

(D) vFB neurons labeled with GFP via conditional expression of GFP using TK-GAL4, nc82 counterstains the brain. Zoomed in view of vFB cell bodies, GFP in green (D'), and TK expression in magenta (D"), (n = 6).

(E and E') Effects of DL1/2-specific knockdown of Imp on vFB neurons. vFB neurons labeled by reporter GFP are shown in green in control (E) and Imp knockdown (17A12-GAL4 > ImpRNAi; ImpRNAi) (E'), nc82 counterstains the brain.

(F-G") Effects of post-mitotic knockdown of Imp on vFB neurons, vFB neurons labeled by reporter GFP are shown in green, Imp expression is shown in magenta in control (F-F") and Imp knockdown (vT029515-GAL4 > ImpRNAi; ImpRNAi) (G-G"). For (F')-(F") and (G')-(G"), the scale bar corresponds to 15 µm.

(H–J) Quantification of the number of cell bodies per hemibrain for type-II-specific knockdown (H), DL1 specific knockdown (I), and post-mitotic knockdown (J). n = data points indicated on the graphs (Student's t test). Asterisks denote levels of significant differences \*p < 0.05; \*\*p < 0.01; \*\*\*p < 0.001; \*\*\*\*p < 0.001. The abbreviated genotypes are shown at the left and top, respectively. Scale bars correspond to 30 µm (unless stated otherwise). The dashed outline shows FB in (A)-(C") and cell bodies in (D')-(D"), (F"), and (G").

See also Figures S1-S4 and Table 1.



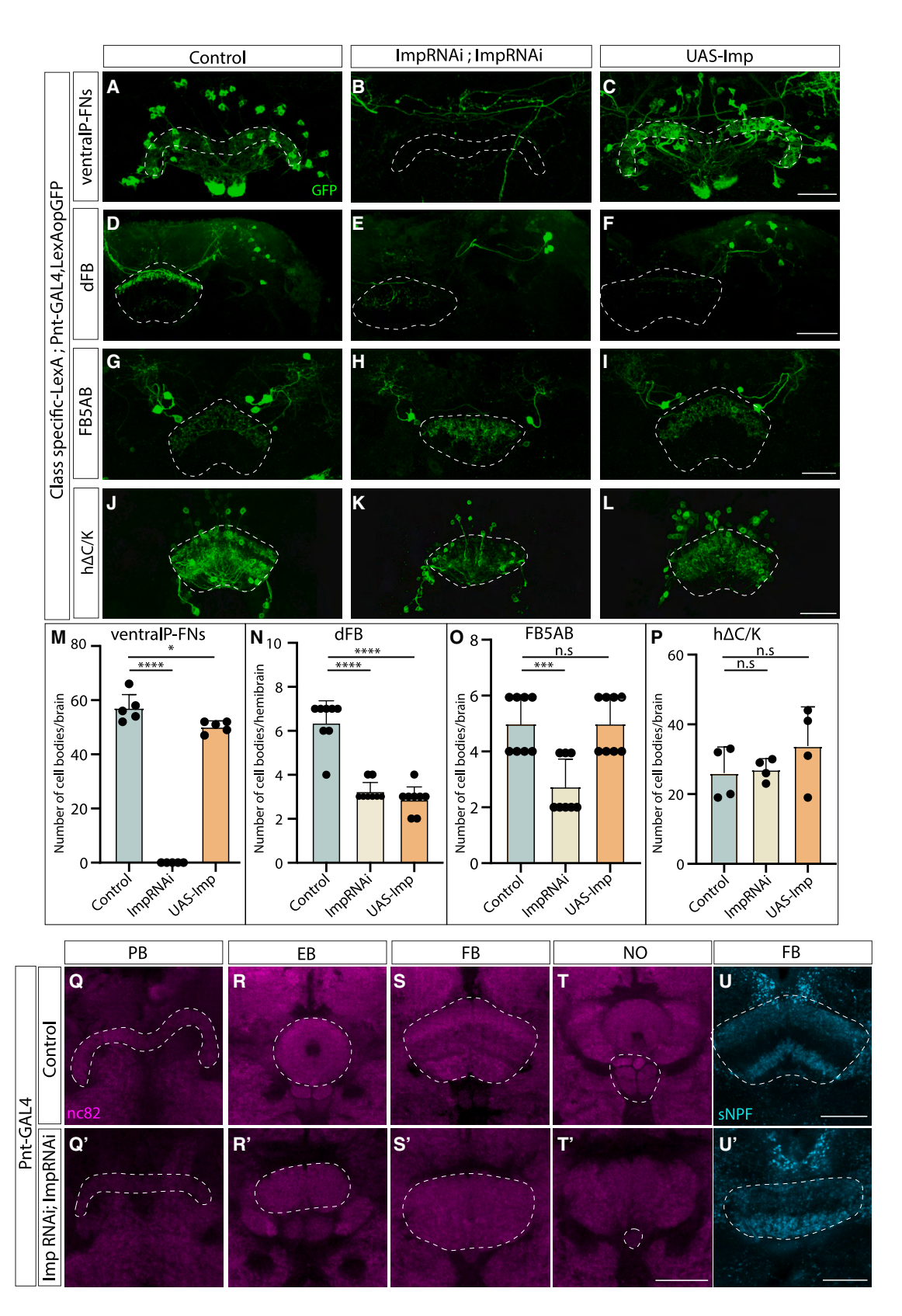


Figure 5. Imp regulates specification and morphology of other neural types in the olfactory navigation circuit (A–C) Ventral P-FN neurons labeled by reporter GFP shown in control (A), Imp knockdown (pointed-GAL4 > ImpRNAi; ImpRNAi) (B), and Imp overexpression (pointed-GAL4 > UAS-Imp) (C).





flies (Figure 6D). In contrast, the distribution of groundspeeds during odor (for moving flies) was not substantially different for Imp KD flies versus controls (Figure 6E). The trajectories of Imp KD flies also showed pronounced zig-zagging (Figure 6B) highlighted by a greater average angular velocity (Figure 6C) and a greater probability of making large amplitude turns (Figure 6F). This suggests that, in the absence of Imp, flies make more larger turns and have difficulty maintaining a stable heading.

Because Imp KD in type II NSCs has broad effects on CX morphology (Figures 5Q-5T"), we next performed a series of control experiments to determine the specificity of behavioral deficits. We first asked whether we could also see behavioral deficits when knocking down Imp only in the DL1/DL2 type II NSCs. This manipulation decreases the number of vFB neurons (Figures 4E and 4E') while leaving overall CX morphology intact (Figure S3). This manipulation also reduced both upwind orientation and average groundspeed during odor (Figures 6G and 6H), suggesting that a narrower manipulation also impacts olfactory behavior. We also asked if we could see behavioral deficits when knocking down a different late-expressed RBP, Syp, which regulates Imp expression in type II NSCs. KD of Syp in type II NSCs was previously shown to produce similar anatomical phenotypes to Imp overexpression<sup>74</sup>; however, we found that it did not affect vFB neuron number (Figures S2A-S2C). KD of Syp produced no change in upwind velocity in response to 1% ACV but produced an increase in upwind velocity in response to 10% ACV (Figure 6J), consistent with the idea that Imp and Syp produce opposing anatomical effects.<sup>74</sup> Finally, we repeated our experiments using a single ImpRNAi transgene, which also results in a complete loss of vFB neurons (Figures S2D-S2F) and using a higher concentration of odor (10% versus 1% apple cider vinegar). In both cases, we observed similar effects of Imp KD on behavior (Figure 6J). We saw no change in upwind velocity modulation in parental strains (pointed-GAL4 or ImpRNAi) crossed to wild type.

To further determine whether the behavioral phenotypes we observed arise from CX deficits, we examined the effects of Imp KD on elements of olfactory navigation circuitry up- and downstream of the CX. We examined three neuron types that have previously been implicated in olfactory navigation or locomotion. Lateral horn output neurons (LH-ONs) known as LHAD1b2<sup>86</sup> and mushroom body output neurons (MBONs) known as MBON-12<sup>87</sup> both respond to odor and drive strong upwind movement. <sup>43</sup> Descending neurons (DNs) known as DNp09 are known to drive changes in forward velocity and turning when activated. <sup>88</sup> Knocking down Imp in type II NSCs had no effect on

any of these neuron types. The neuron number and morphology of LH-ONs labeled by 55C09-LexA, MBONs labeled by 25D01-LexA, and DNs labeled by 38F04-LexA were unaltered (Figure S4; Table 1). nc82 stains also show that MB morphology is normal in type II > ImpRNAi flies (Videos S2 and S3). Although not fully conclusive, these data support the idea that the behavioral phenotype we observe arises majorly from CX deficits.

#### **DISCUSSION**

During development, NSCs generate diverse neuron types that assemble into distinct neural circuits enabling complex behaviors. Extensive work in genetic model systems has provided an overview of conserved temporal programs that govern the formation of diverse neuronal cell types. 63,65,89-91 Although much is now known about the stem cell-specific molecular cues that determine cell type identity, understanding how these molecular cues shape the expression of complex behaviors is still in its infancy. 92-94 The insect CX provides an ideal model for dissecting the relationship between developmental processes and behavioral complexity. The majority of Drosophila CX neurons are derived from a few type II NSCs, which follow a division program similar to that of cortical progenitors. 58,59,62-65 The CX has been implicated in a number of behaviors that include olfactory navigation, 43 menotaxis, 23,45 sleep 30-32 and path integration in Drosophila, 95-97 and species-specific behaviors, such as longdistance migration, in monarch butterflies, 98 and allocentric dispersion in dung beetles.99 For these reasons, the insect CX provides an ideal model for dissecting the relationship between developmental processes and behavioral complexity.

### Lineage-specific developmental plan of the CX neuron types

Lineage-based architecture plays an essential role in generating complex brain structures and circuits. In the mammalian cerebral cortex, lineage is known to regulate neuron connectivity, where excitatory neurons originating from the same progenitors process related information and connect with each other, and inhibitory neurons are also known to organize in a lineage-dependent manner. <sup>100,101</sup> In the *Drosophila* larval ventral nerve cord (VNC), different lineages were reported to assemble with the sequential addition of temporal cohorts where circuit output neurons are born before circuit input neurons. <sup>102</sup> In the CX, local and columnar neurons primarily arise from the DM lineages (DM1–4), whereas long-field tangential input neurons arise from a variety of lineages. <sup>51,55</sup> One prominent cluster primarily

(D–F) dFB (65C03) neurons labeled by reporter GFP shown in control (D), Imp knockdown (pointed-GAL4 > ImpRNAi; ImpRNAi) with defective morphology of the neurites in FB (E), and Imp overexpression (pointed-GAL4 > UAS-Imp) (F).

<sup>(</sup>G-I) FB5AB input neurons labeled by reporter GFP in control (G), Imp knockdown (pointed-GAL4 > ImpRNAi; ImpRNAi) with defective morphology of the neurites in FB (H), and Imp overexpression (pointed-GAL4 > UAS-Imp) (I).

<sup>(</sup>J-L) h $\Delta$ C/K neurons labeled by reporter GFP in control (J), neurites arborize multiple layers of FB with no clear demarcation in Imp knockdown (pointed-GAL4 > ImpRNAi; ImpRNAi) (K) and Imp overexpression (pointed-GAL4 > UAS-Imp) (L). GFP is shown in green, the abbreviated genotypes are shown at left and top. Scale bars correspond to 30  $\mu$ m.

<sup>(</sup>M–P) Quantification of number of cell bodies. Abbreviated neuron names are indicated at the top. n = data points indicated on the graphs (Student's t test). Asterisks denote levels of significant differences: \*p < 0.05; \*\*p < 0.01; \*\*\*p < 0.001; \*\*\*\*p < 0.0001.

<sup>(</sup>Q-U') The four neuropils of the CX: PB, NO, FB, and EB in control flies (Q-T), and Imp knockdown resulting in defective morphology of the CX neuropils (Q'-T'). nc82 stains the neuropils of the brain, all outlined using dashed lines, (n = 22). (U and U') sNPF stains shown in cyan in control distributed in dorsal and ventral layers of FB distinctly (U), and Imp knockdown shows impaired distribution (U'). Scale bars correspond to 30  $\mu$ m. See also Figures S2 and S4 and Videos S2 and S3.



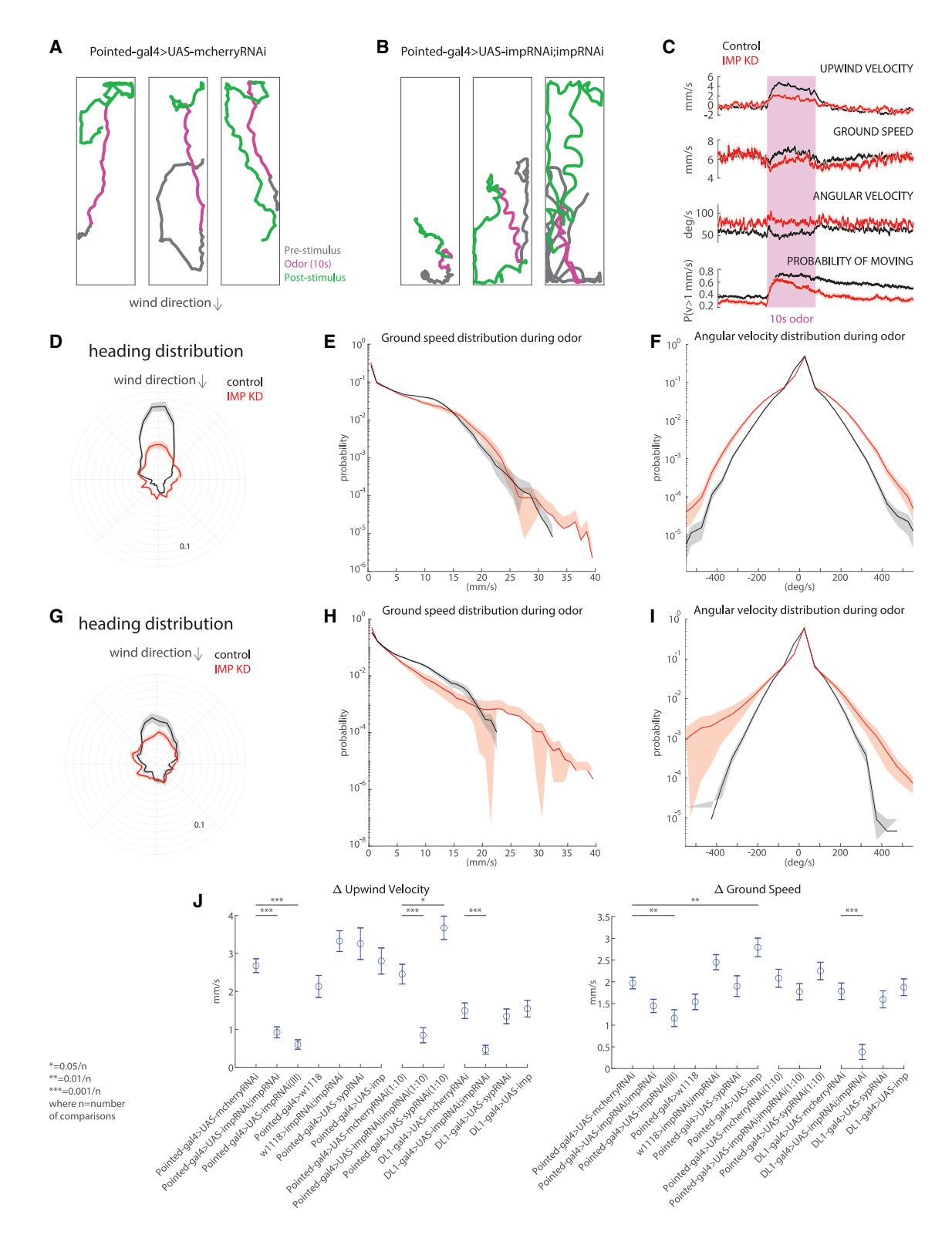


Figure 6. Imp regulates the upwind orientation during olfactory navigation

(A) Representative walking trajectories of three different control flies (pointed-GAL4 > UASmCherryRNAi) presented with a 10 s odor pulse (1% ACV, magenta) centered in a 70 s trial with 10 cm/s wind. Flies demonstrate upwind movement during odor and local search after odor offset. Wind direction indicated.

(B) Representative walking trajectories of three different Imp knockdown flies (pointed-GAL4 > UAS-ImpRNAi; UAS-ImpRNAi) in the same wind and odor conditions as (A). Trajectories reveal lack of upwind movement during odor and increased turning behavior throughout the entirety of trial.





arises from the DL type II lineage (DL1) and generates neurons that fasciculate in two distinct bundles, one innervating the dorsal and the other ventral layers of the FB. However, many other type I lineages also generate long-field tangential inputs, including AOTU, LALv1, and SIPp1.51,55

Here, we show that the major components of a previously described olfactory navigation circuit in the CX are all derived from type II NSCs (Figure 2). Although many odor-encoding input neurons (vFB) are born from DL1 NSCs, a few are derived from other DMs (Figure 3). Our clonal analysis revealed that, although tangential input neurons look morphologically similar, they can be derived from different lineages. Based on our genetic birthdating results, we found that the neurons that innervate the ventral layers and provide odor input to the navigation circuits are born between 48 and 72 h ALH (Figure 3). Our findings align with birth-dating studies on the entire DL1 lineage, which revealed that the ventral projecting neurons are born before 72 h ALH and that the dorsal projecting neurons are born throughout larval development. 74 Our studies indicate that components of a functional circuit associated with a behavior in CX are derived from multiple lineages and assembled over time. It will be intriguing to investigate whether other elements of the circuit are born at the same or different times. Whether other insects share a similar lineage-based circuit architecture and assembly will be interesting to pursue.

#### Role of Imp in specifying an olfactory navigation circuit

Imp has previously been shown to be important in neuronal development and specification. In mice, loss of Imp leads to deformities in the posterior brain, neuroepithelial orientation defects, and cellular packing deficiency with poorly defined barriers between cortical layers/zones,85 similar to the overall defective morphology and lamination defects we observe in the CX. Temporal gradients of two RBPs, Imp and Syp, have

been shown to determine neural identity in the insect mushroom body, antennal lobe, and CX.74,103 In mushroom body neuroblasts, high Imp/low Syp levels early in development promote the specification of early-born  $\gamma$  Kenyon cells, whereas low Imp/high Syp levels late in development promote the specification of late-born  $\alpha/\beta$  Kenyon cells. In mushroom body neuroblasts, Imp was shown to regulate fate of neuronal subtypes partly via regulating the translation of transcription factor Chinmo, 103-105 suggesting that Imp governs fate by regulating the expression of other temporal transcription factors. In the antennal lobe, high Imp/low Syp leads to an increased number of late-born neurons from the antennal lobe antero-dorsal 1 (ALad1) lineage at the expense of early-born ones. 103 In the type II lineages, DM1 and DL1 Imp/Syp levels control the number of several cell types.<sup>74</sup> However, the effects of these RBPs on multiple components of a functional circuit have not been previously characterized.

Here, focusing on an olfactory navigation circuit within the CX, we found the strongest effects of Imp on neurons targeting the vFB-ventral tangential inputs and ventral P-FNs. Curiously, Imp levels had distinct effects on each circuit element. In some cases (such as vFB neurons), KD of Imp caused a reduction in neuron number, whereas overexpression caused an increase in neuronal number (Figure 4), supporting existing models that Imp expression promotes the specification of neurons normally born in a particular temporal window. 74,103 However, for other neurons, we observed diverse effects of KD and overexpression (Figure 5). These observations suggest that precise levels of Imp are required to specify the correct number of these neurons, and Imp might be acting differently in type II NSCs and in combination with other NSC factors or INP factors to give rise to different cell types. Imp may play multiple roles and act via different molecular mechanisms in the NSCs to specify distinct neuron types from distinct lineages. We further show that the expression of

(C) Comparison of movement parameters between control (black, n = 86 flies) and Imp knockdown flies (red, n = 61 flies) calculated as an average across flies (mean ± SEM; see STAR Methods). Pink-shaded area: 10-s odor stimulation period (1% ACV). In the presence of odor, Imp knockdown flies show decreased upwind velocity comparable to control flies. Increased turning behavior noted in (B) can be observed quantitatively through the increased angular velocity throughout the duration of trials.

(J) Change in upwind velocity and ground speed, calculated as the difference in the mean value during the first 5 s of odor and the 5 s preceding odor, across various control and experimental genotypes. Knockdown of Imp results in significant decreases in upwind velocity change when compared with respective controls, across multiple odor strengths and driver lines (pointed-GAL4 > mCherryRNAi compared with pointed > double ImpRNAi p = 5.906 × 10<sup>-11</sup>, pointed-GAL4 > mCherryRNAi compared with pointed-GAL4 > ImpRNAi(III) p = 1.14768 × 10<sup>-9</sup>, pointed-GAL4 > mCherryRNAi (1:10 AVC) compared with pointed-GAL4 > double ImpRNAi (10:1) p = 1.2293 × 10<sup>-4</sup>, DL1 > mCherry compared with DL1 > double ImpRNAi p = 9.922 × 10<sup>-6</sup>). Knockdown of late transcription factor Syncrip (Syp) results in a significant increase in upwind velocity when using a higher odor concentration (1:10 ACV, pointed-GAL4 > mCherryRNAi compared with pointed-GAL4 > SypRNAi [10:1] p = 0.0042). Knockdown of Imp using a single copy of the RNAi results in a significant decrease in ground speed (pointed-GAL4 > mCherryRNAi compared with pointed-GAL4 > ImpRNAi; [III] p = 0.0015), as does knockdown in DL1/DL2 type II NSCs (17A12-GAL4 > ImpRNAi; ImpRNAi, two-sample t test; p = 2.2281 × 10<sup>-7</sup>). Upregulation of Imp results in increased ground speed but no change to upwind velocity (pointed-GAL4 > mCherryRNAi compared with pointed-GAL4 > UAS-Imp p = 7.7113 × 10<sup>-4</sup>). All comparisons were completed using an unpaired t test with Bonferroni correction for multiple comparisons.

See also Figures 4, S1, and S2.

<sup>(</sup>D) Heading distribution during odor for both control (black) and Imp knockdown (red) flies (wind direction indicated above). Imp knockdown flies exhibit decreased upwind orientation.

<sup>(</sup>E) Histogram showing ground speed distributions during odor for both control (black) and Imp knockdown (red). Distributions appear similar, suggesting that general movement is not impaired by Imp knockdown.

<sup>(</sup>F) Histogram showing angular velocity distributions for both control (black) and Imp knockdown flies (red) during odor. Imp knockdown flies favor larger angular velocities, even in the presence of an attractive stimulus.

<sup>(</sup>G) Heading distribution during odor for both control (black) and knockdown of Imp (red) in DL1/2 type II NSCs (wind direction indicated by above arrow).

<sup>(</sup>H) Histogram showing ground speed distribution during odor for both control (black) and Imp knockdown (red) flies. Imp knockdown flies tend toward lower ground speeds than control counterparts.

<sup>(</sup>I) Histogram showing angular velocity distribution during odor for both control (black) and Imp knockdown (red) flies. Widening of distribution indicates that Imp knockdown flies favor larger angular velocities.





Imp post mitotically in vFB neurons maintains their identity (Figure 4G). Moreover, we find that manipulating Imp levels in type II NSCs affects the morphology of CX neuropils and distributions of neuropeptides TK and sNPF, throughout the FB (Figures 4 and 5). These studies provide the first insights into the relationship between developmental timing and establishing neuropeptidergic identity in CX.

An open question is how Imp regulates neural fate and the function of multiple circuit elements at the molecular level. Imp was previously shown to regulate fate specification by regulating the translation of transcription factor Chinmo. 103-105 Previous studies have shown that Chinmo is persistently expressed in type II NSCs that are mutant for Syp and thus maintain high Imp expression throughout development, and this manipulation resulted in the formation of extra early-born neuron types. 73,74 This suggests the underlying mechanism to be the regulation of the expression of other transcription factors. However, we cannot rule out the possibility of Imp regulating cell fate directly. RBPs are known to play essential roles in regulating temporal gene expression by affecting the stability and translation of mRNA. 103 In the VNC motor neuron lineage. LinA/15, Imp, and Syp regulate axon-muscle connectivity by regulating various transcription factors post-transcriptionally. 106 Previous work has also shown a role for Imp in the timing of NSC quiescence and proliferation. 83,107 Because many other neural cell types that arise from type II NSCs are not affected upon Imp KD, we conclude that the phenotypes we observe are less likely to be associated with quiescence or cell proliferation. RBPs can regulate gene expression by creating liquid phase separation granules. Imp has intrinsically disordered domains and is known to promote phase separation in mushroom body neurons. 108 Whether Imp makes phase-separated granules in type II NSCs and if that has a role in fate specification is not known. Future studies will elaborate on the different molecular mechanisms underlying the effect of Imp on multiple circuit elements.

#### **Developmental dissection of CX-mediated behavior**

In this study, we showed that KD of the early-expressed RBP Imp in type II NSC lineages largely abolishes upwind orientation in response to odor. We also observed a weaker phenotype when we knocked down Imp, specifically in DL1/DL2 type II NSCs, arguing that tangential inputs to the CX have a specific role in generating this behavior (Figure 6). We did not observe any behavioral deficit with Syp KD in type II NSCs, although this manipulation has previously been shown to significantly impact neuronal specification in the CX.74 Our control experiments suggest that these behavioral deficits are most likely due to alterations to CX structure. However, we cannot be sure that they arise from the changes in circuit structure that we have characterized here, and we cannot rule out a role for type-II-derived neurons outside the CX in the more severe phenotype. Current approaches to CX circuit dissection in fruit flies have emphasized the use of highly specific GAL4 and Split-GAL4 lines, which target specific subsets of neurons. 109,110 Silencing of highly specific CX lines often produces subtle phenotypes. For example, silencing of compass neurons eliminates menotaxis (orientation to a visual stimulus at an angular offset) but not visual fixation per se, <sup>23,111</sup> whereas silencing of hΔC/K neurons impairs the persistence of upwind tracking behavior during odor but not the initial upwind turn. <sup>43</sup> Here, we have shown that developmental manipulation of small groups of stem cells can produce a more striking phenotype, providing a complementary approach to dissecting neural circuits with highly specific driver lines. Future experiments manipulating other temporally expressed transcription factors or intersecting their manipulation with the temporal transcription factor code in INPs should allow us to make more precise manipulations of CX development.

#### **STAR**\*METHODS

Detailed methods are provided in the online version of this paper and include the following:

- KEY RESOURCES TABLE
- RESOURCE AVAILABILITY
  - Lead contact
  - Materials availability
  - Data and code availability
- EXPERIMENTAL MODEL AND STUDY PARTICIPANT DETAILS
- METHOD DETAILS
  - Immunostaining
  - Microscopy
  - Birth-dating using Cell class lineage intersection system
  - Behavioral Apparatus
- QUANTIFICATION AND STATISTICAL ANALYSIS
  - Analysis of Behavioral Data
  - Orientation histograms
  - O Histograms of ground speed and angular velocity
  - Summary plots of change in forward velocity and ground speed

#### SUPPLEMENTAL INFORMATION

Supplemental information can be found online at https://doi.org/10.1016/j.cub.2023.12.020.

#### **ACKNOWLEDGMENTS**

The authors would like to thank Chris Doe and Doe lab members for their valuable feedback and discussions. We thank Gonzalo Morales Chaya for the 17A12GAL4 expression image and Adil Wani for the 17A12GAL4, Lex-AopmCD8GFP fly. We thank Chris Doe, Raees Andrabi, and Dena Goldblatt for providing critical feedback on the manuscript. We are grateful to Chris Doe, Claude Desplan, Gerry Rubin, Jan Veenstra, and Tzumin Lee for sharing the reagents. We thank Gerry Rubin and Heather Dionne for plasmids for VT062617 and VT029515, which we used to generate LexA lines. Stocks obtained from the Bloomington Drosophila Stock Center (NIH P400D018537) were used in this study. The monoclonal nc82 antibody was obtained from the Developmental Studies Hybridoma Bank, created by the NICHD of the NIH and maintained at The University of Iowa, Department of Biology, Iowa City, IA 52242. We thank University of New Mexico Biology cell biology core for providing confocal microscopy facility. We thank the Advanced Imaging Core facility at Janelia Research Campus used for the experiments conducted during the revision of this manuscript. The ideas that partly influenced this research came from discussions at the KITP Neurophysics of Locomition Program in 2022 supported by NSF-PHY-1748958 and the Gordon and Betty Moore Foundation grant no. 2919.02. A.N.C. was supported by NIH MARC





T34GM008751, and A.G. was supported by NIH URISE T34 GM145428. The research was supported by NSF 2014217, NIH R01DC017979, and RF1NS127129 to K.N. and University of New Mexico College of Arts & Sciences Office of Research, Sloan Research Fellowship grant number FG-2023-20617, and National Science Foundation CAREER award IOS-2047020 to M.H.S.

#### **AUTHOR CONTRIBUTIONS**

Conceptualization, A.H., K.N., and M.H.S.; methodology, A.H. performed all anatomy experiments and confocal imaging; A.G. helped in confirming the TK-GAL4 line expression; H.G., A.N.C., M.P., and T.S. performed behavior experiments; visualization, A.H., K.N., and M.H.S.; writing, A.H.; editing, K.N. and M.H.S.; funding acquisition, K.G. and M.H.S.; supervision, K.N. and M.H.S.

#### **DECLARATION OF INTERESTS**

The authors declare no competing interests.

#### **INCLUSION AND DIVERSITY**

One or more of the authors of this paper self-identifies as an underrepresented ethnic minority in their field of research or within their geographical location.

Received: May 19, 2023 Revised: November 14, 2023 Accepted: December 7, 2023 Published: January 4, 2024

#### **REFERENCES**

- Rubenstein, J.L. (2010). Three hypotheses for developmental defects that may underlie some forms of autism spectrum disorder. Curr. Opin. Neurol. 23, 118–123.
- Guerrini, R., Dobyns, W.B., and Barkovich, A.J. (2008). Abnormal development of the human cerebral cortex: genetics, functional consequences and treatment options. Trends Neurosci. 31, 154–162.
- Gilbert, S.L., Dobyns, W.B., and Lahn, B.T. (2005). Genetic links between brain development and brain evolution. Nat. Rev. Genet. 6, 581–590.
- Farris, S.M., and Sinakevitch, I. (2003). Development and evolution of the insect mushroom bodies: towards the understanding of conserved developmental mechanisms in a higher brain center. Arthropod Struct. Dev. 32, 79–101.
- 5. Strausfeld, N.J. (1976). Atlas of an Insect Brain (Springer).
- Honkanen, A., Adden, A., da Silva Freitas, J.da S., and Heinze, S. (2019).
   The insect central complex and the neural basis of navigational strategies. J. Exp. Biol. 222.
- 7. Homberg, U. (1985). Interneurones of the central complex in the bee brain (Apis mellifera, L.). J. Insect Physiol. *31*, 251–264.
- Strauss, R., and Heisenberg, M. (1993). A higher control center of locomotor behavior in the Drosophila brain. J. Neurosci. 13, 1852–1861.
- Homberg, U. (2004). In search of the sky compass in the insect brain. Naturwissenschaften 91, 199–208.
- Wessnitzer, J., and Webb, B. (2006). Multimodal sensory integration in insects—towards insect brain control architectures. Bioinspir Biomim 1, 63–75.
- Homberg, U. (2008). Evolution of the central complex in the arthropod brain with respect to the visual system. Arthropod Struct. Dev. 37, 347–362
- 12. Strausfeld, N.J. (2009). Brain organization and the origin of insects: an assessment. Proc. Biol. Sci. 276, 1929–1937.
- Ofstad, T.A., Zuker, C.S., and Reiser, M.B. (2011). Visual place learning in Drosophila melanogaster. Nature 474, 204–207.
- Pfeiffer, K., and Homberg, U. (2014). Organization and functional roles of the central complex in the insect brain. Annu. Rev. Entomol. 59, 165–184.

- Seelig, J.D., and Jayaraman, V. (2015). Neural dynamics for landmark orientation and angular path integration. Nature 521, 186–191.
- Turner-Evans, D., Wegener, S., Rouault, H., Franconville, R., Wolff, T., Seelig, J.D., Druckmann, S., and Jayaraman, V. (2017). Angular velocity integration in a fly heading circuit. eLife 6, e23496.
- Green, J., Adachi, A., Shah, K.K., Hirokawa, J.D., Magani, P.S., and Maimon, G. (2017). A neural circuit architecture for angular integration in Drosophila. Nature 546, 101–106.
- Turner-Evans, D.B., Jensen, K.T., Ali, S., Paterson, T., Sheridan, A., Ray, R.P., Wolff, T., Lauritzen, J.S., Rubin, G.M., Bock, D.D., et al. (2020). The neuroanatomical ultrastructure and function of a biological ring attractor. Neuron 108, 145–163.e10.
- Behbahani, A.H., Palmer, E.H., Corfas, R.A., and Dickinson, M.H. (2021).
   Drosophila re-zero their path integrator at the center of a fictive food patch. Curr. Biol. 31, 4534–4546.e5.
- Lyu, C., Abbott, L.F., and Maimon, G. (2022). Building an allocentric travelling direction signal via vector computation. Nature 601, 92–97.
- Lu, J., Behbahani, A.H., Hamburg, L., Westeinde, E.A., Dawson, P.M., Lyu, C., Maimon, G., Dickinson, M.H., Druckmann, S., and Wilson, R.I. (2022). Transforming representations of movement from body- to world-centric space. Nature 601, 98–104.
- Neuser, K., Triphan, T., Mronz, M., Poeck, B., and Strauss, R. (2008).
   Analysis of a spatial orientation memory in Drosophila. Nature 453, 1244–1247.
- Giraldo, Y.M., Leitch, K.J., Ros, I.G., Warren, T.L., Weir, P.T., and Dickinson, M.H. (2018). Sun navigation requires compass neurons in Drosophila. Curr. Biol. 28, 2845–2852.e4.
- Dan, C., Kappagantula, R., Hulse, B.K., Jayaraman, V., and Hermundstad, A.M. (2022). Flexible control of behavioral variability mediated by an internal representation of head direction. https://doi.org/10. 1101/2021.08.18.456004.
- Martin, J.P., Guo, P., Mu, L., Harley, C.M., and Ritzmann, R.E. (2015).
   Central-complex control of movement in the freely walking cockroach.
   Curr. Biol. 25, 2795–2803.
- Rayshubskiy, A., Holtz, S.L., D'Alessandro, I., Li, A.A., Vanderbeck, Q.X., Haber, I.S., Gibb, P.W., and Wilson, R.I. (2020). Neural circuit mechanisms for steering control in walking Drosophila. https://doi.org/10. 1101/2020.04.04.024703.
- Musso, P.-Y., Junca, P., and Gordon, M.D. (2021). A neural circuit linking two sugar sensors regulates satiety-dependent fructose drive in Drosophila. Sci. Adv. 7, eabj0186.
- Sareen, P.F., McCurdy, L.Y., and Nitabach, M.N. (2021). A neuronal ensemble encoding adaptive choice during sensory conflict in Drosophila. Nat. Commun. 12, 4131.
- Ishimoto, H., and Kamikouchi, A. (2020). A feedforward circuit regulates action selection of pre-mating courtship behavior in female Drosophila. Curr. Biol. 30, 396–407.e4.
- Donlea, J.M., Thimgan, M.S., Suzuki, Y., Gottschalk, L., and Shaw, P.J. (2011). Inducing sleep by remote control facilitates memory consolidation in Drosophila. Science 332, 1571–1576.
- 31. Donlea, J.M., Pimentel, D., and Miesenböck, G. (2014). Neuronal machinery of sleep homeostasis in Drosophila. Neuron 81, 860–872.
- Donlea, J.M., Pimentel, D., Talbot, C.B., Kempf, A., Omoto, J.J., Hartenstein, V., and Miesenböck, G. (2018). Recurrent circuitry for balancing sleep need and sleep. Neuron 97, 378–389.e4.
- 33. Liu, S., Liu, Q., Tabuchi, M., and Wu, M.N. (2016). Sleep drive is encoded by neural plastic changes in a dedicated circuit. Cell 165, 1347–1360.
- Dubowy, C., and Sehgal, A. (2017). Circadian rhythms and sleep in Drosophila melanogaster. Genetics 205, 1373–1397.
- Kempf, A., Song, S.M., Talbot, C.B., and Miesenböck, G. (2019). A potassium channel β-subunit couples mitochondrial electron transport to sleep. Nature 568, 230–234.

#### **Article**



- Chakravarti Dilley, L., Szuperak, M., Gong, N.N., Williams, C.E., Saldana, R.L., Garbe, D.S., Syed, M.H., Jain, R., and Kayser, M.S. (2020). Identification of a molecular basis for the juvenile sleep state. eLife 9, e52676.
- Shafer, O.T., and Keene, A.C. (2021). The regulation of drosophila sleep. Curr. Biol. 31, R38–R49.
- Hanesch, U., Fischbach, K.-F., and Heisenberg, M. (1989). Neuronal architecture of the central complex in *Drosophila melanogaster*. Cell Tissue Res. 257, 343–366.
- Ito, K., Shinomiya, K., Ito, M., Armstrong, J.D., Boyan, G., Hartenstein, V., Harzsch, S., Heisenberg, M., Homberg, U., Jenett, A., et al. (2014). A systematic nomenclature for the insect brain. Neuron 81, 755–765.
- Wolff, T., Iyer, N.A., and Rubin, G.M. (2015). Neuroarchitecture and neuroanatomy of the *Drosophila* central complex: a GAL4-based dissection of protocerebral bridge neurons and circuits. J. Comp. Neurol. 523, 997–1037.
- Wolff, T., and Rubin, G.M. (2018). Neuroarchitecture of the Drosophila central complex: A catalog of nodulus and asymmetrical body neurons and a revision of the protocerebral bridge catalog. J. Comp. Neurol. 526 2585–2611
- Álvarez-Salvado, E., Licata, A.M., Connor, E.G., McHugh, M.K., King, B.M., Stavropoulos, N., Victor, J.D., Crimaldi, J.P., and Nagel, K.I. (2018). Elementary sensory-motor transformations underlying olfactory navigation in walking fruit-flies. eLife 7, e37815.
- Matheson, A.M.M., Lanz, A.J., Medina, A.M., Licata, A.M., Currier, T.A., Syed, M.H., and Nagel, K.I. (2022). A neural circuit for wind-guided olfactory navigation. Nat. Commun. 13, 4613.
- Franconville, R., Beron, C., and Jayaraman, V. (2018). Building a functional connectome of the Drosophila central complex. eLife 7, e37017.
- Green, J., and Maimon, G. (2018). Building a heading signal from anatomically defined neuron types in the Drosophila central complex. Curr. Opin. Neurobiol. 52, 156–164.
- Pires, P.M., Abbott, L.F., and Maimon, G. (2022). Converting an allocentric goal into an egocentric steering signal. https://doi.org/10.1101/2022.
   11.10.516026
- Currier, T.A., Matheson, A.M., and Nagel, K.I. (2020). Encoding and control of orientation to airflow by a set of Drosophila fan-shaped body neurons. eLife 9. e61510.
- 48. Hulse, B.K., Haberkern, H., Franconville, R., Turner-Evans, D.B., Takemura, S.Y., Wolff, T., Noorman, M., Dreher, M., Dan, C., Parekh, R., et al. (2021). A connectome of the Drosophila central complex reveals network motifs suitable for flexible navigation and context-dependent action selection. eLife 10, e66039.
- Scheffer, L.K., Xu, C.S., Januszewski, M., Lu, Z., Takemura, S.-Y., Hayworth, K.J., Huang, G.B., Shinomiya, K., Maitlin-Shepard, J., Berg, S., et al. (2020). A connectome and analysis of the adult Drosophila central brain. eLife 9, e57443.
- Sayre, M.E., Templin, R., Chavez, J., Kempenaers, J., and Heinze, S. (2021). A projectome of the bumblebee central complex. eLife 10, e68911.
- Yang, J.S., Awasaki, T., Yu, H.-H., He, Y., Ding, P., Kao, J.-C., and Lee, T. (2013). Diverse neuronal lineages make stereotyped contributions to the Drosophila locomotor control center, the central complex. J. Comp. Neurol. 521, 2645–Spc1.
- Yu, H.-H., Awasaki, T., Schroeder, M.D., Long, F., Yang, J.S., He, Y., Ding, P., Kao, J.-C., Wu, G.Y.-Y., Peng, H., et al. (2013). Clonal development and organization of the adult Drosophila central brain. Curr. Biol. 23, 633–643.
- 53. Ito, M., Masuda, N., Shinomiya, K., Endo, K., and Ito, K. (2013). Systematic analysis of neural projections reveals clonal composition of the Drosophila brain. Curr. Biol. 23, 644–655.
- Pereanu, W., Kumar, A., Jennett, A., Reichert, H., and Hartenstein, V. (2010). Development-based compartmentalization of the Drosophila central brain. J. Comp. Neurol. 518, 2996–3023.

- Kandimalla, P., Omoto, J.J., Hong, E.J., and Hartenstein, V. (2023).
   Lineages to circuits: the developmental and evolutionary architecture of information channels into the central complex. J. Comp. Physiol. A Neuroethol. Sens. Neural Behav. Physiol. 209, 679–720.
- Homem, C.C.F., and Knoblich, J.A. (2012). Drosophila neuroblasts: a model for stem cell biology. Development 139, 4297–4310.
- Hamid, A., Gutierrez, A., Munroe, J., and Syed, M.H. (2023). The Drivers of Diversity: integrated genetic and hormonal cues regulate neural diversity. Semin. Cell Dev. Biol. 142, 23–35.
- Bello, B.C., Izergina, N., Caussinus, E., and Reichert, H. (2008).
   Amplification of neural stem cell proliferation by intermediate progenitor cells in *Drosophila* brain development. Neural Dev. 3, 5.
- Boone, J.Q., and Doe, C.Q. (2008). Identification of *Drosophila* type II neuroblast lineages containing transit amplifying ganglion mother cells. Dev. Neurobiol. 68, 1185–1195.
- Bowman, S.K., Rolland, V., Betschinger, J., Kinsey, K.A., Emery, G., and Knoblich, J.A. (2008). The tumor suppressors Brat and Numb regulate transit-amplifying neuroblast lineages in *Drosophila*. Dev. Cell 14, 535–546.
- Izergina, N., Balmer, J., Bello, B., and Reichert, H. (2009). Postembryonic development of transit amplifying neuroblast lineages in the Drosophila brain. Neural Dev. 4, 44.
- Jiang, Y., and Reichert, H. (2013). Analysis of neural stem cell selfrenewal and differentiation by transgenic RNAi in Drosophila. Arch. Biochem. Biophys. 534, 38–43.
- Oberst, P., Agirman, G., and Jabaudon, D. (2019). Principles of progenitor temporal patterning in the developing invertebrate and vertebrate nervous system. Curr. Opin. Neurobiol. 56, 185–193.
- **64.** Florio, M., and Huttner, W.B. (2014). Neural progenitors, neurogenesis and the evolution of the neocortex. Development *141*, 2182–2194.
- Lodato, S., and Arlotta, P. (2015). Generating neuronal diversity in the mammalian cerebral cortex. Annu. Rev. Cell Dev. Biol. 31, 699–720.
- Hansen, D.V., Lui, J.H., Parker, P.R.L., and Kriegstein, A.R. (2010).
   Neurogenic radial glia in the outer subventricular zone of human neocortex. Nature 464, 554–561.
- 67. Lui, J.H., Hansen, D.V., and Kriegstein, A.R. (2011). Development and evolution of the human neocortex. Cell *146*, 18–36.
- Pebworth, M.-P., Ross, J., Andrews, M., Bhaduri, A., and Kriegstein, A.R. (2021). Human intermediate progenitor diversity during cortical development. Proc. Natl. Acad. Sci. USA *118*, e2019415118.
- 69. Williams, J.L.D., and Boyan, G.S. (2008). Building the central complex of the grasshopper Schistocerca gregaria: axons pioneering the w, x, y, z tracts project onto the primary commissural fascicle of the brain. Arthropod Struct. Dev. 37, 129–140.
- Boyan, G.S., and Reichert, H. (2011). Mechanisms for complexity in the brain: generating the insect central complex. Trends Neurosci. 34, 247–257
- Boyan, G., Liu, Y., Khalsa, S.K., and Hartenstein, V. (2017). A conserved plan for wiring up the fan-shaped body in the grasshopper and Drosophila. Dev. Genes Evol. 227, 253–269.
- 72. He, B., Buescher, M., Farnworth, M.S., Strobl, F., Stelzer, E.H., Koniszewski, N.D., Muehlen, D., and Bucher, G. (2019). An ancestral apical brain region contributes to the central complex under the control of foxQ2 in the beetle Tribolium. eLife 8, e49065.
- Syed, M.H., Mark, B., and Doe, C.Q. (2017). Steroid hormone induction of temporal gene expression in Drosophila brain neuroblasts generates neuronal and glial diversity. eLife 6, e26287.
- 74. Ren, Q., Yang, C.-P., Liu, Z., Sugino, K., Mok, K., He, Y., Ito, M., Nern, A., Otsuna, H., and Lee, T. (2017). Stem cell-intrinsic, seven-up-triggered temporal factor gradients diversify intermediate neural progenitors. Curr. Biol. 27, 1303–1313.
- Wang, Y.-C., Yang, J.S., Johnston, R., Ren, Q., Lee, Y.-J., Luan, H., Brody, T., Odenwald, W.F., and Lee, T. (2014). Drosophila intermediate





- neural progenitors produce lineage-dependent related series of diverse neurons. Development 141, 253–258.
- Abdusselamoglu, M.D., Eroglu, E., Burkard, T.R., and Knoblich, J.A. (2019). The transcription factor odd-paired regulates temporal identity in transit-amplifying neural progenitors via an incoherent feed-forward loop, eLife 8, e46566.
- Tang, J.L.Y., Hakes, A.E., Krautz, R., Suzuki, T., Contreras, E.G., Fox, P.M., and Brand, A.H. (2021). NanoDam identifies novel temporal transcription factors conserved between the Drosophila central brain and visual system. https://doi.org/10.1101/2021.06.07.447332.
- Bayraktar, O.A., and Doe, C.Q. (2013). Combinatorial temporal patterning in progenitors expands neural diversity. Nature 498, 449–455.
- Demir, M., Kadakia, N., Anderson, H.D., Clark, D.A., and Emonet, T. (2020). Walking Drosophila navigate complex plumes using stochastic decisions biased by the timing of odor encounters. eLife 9, e57524.
- Steele, T.J., Lanz, A.J., and Nagel, K.I. (2023). Olfactory navigation in arthropods. J. Comp. Physiol. A Neuroethol. Sens. Neural Behav. Physiol. 209 467–488
- Ren, Q., Awasaki, T., Huang, Y.-F., Liu, Z., and Lee, T. (2016). Cell classlineage analysis reveals sexually dimorphic lineage compositions in the drosophila brain. Curr. Biol. 26, 2583–2593.
- Degrauwe, N., Suvà, M.-L., Janiszewska, M., Riggi, N., and Stamenkovic, I. (2016). IMPs: an RNA-binding protein family that provides a link between stem cell maintenance in normal development and cancer. Genes Dev. 30, 2459–2474.
- Munroe, J.A., Syed, M.H., and Doe, C.Q. (2022). Imp is required for timely exit from quiescence in Drosophila type II neuroblasts. PLoS One 17, e0272177.
- Kahsai, L., and Winther, Å.M.E. (2011). Chemical neuroanatomy of the Drosophila central complex: distribution of multiple neuropeptides in relation to neurotransmitters. J. Comp. Neurol. 519, 290–315.
- 85. Núñez, L., Buxbaum, A.R., Katz, Z.B., Lopez-Jones, M., Nwokafor, C., Czaplinski, K., Pan, F., Rosenberg, J., Monday, H.R., and Singer, R.H. (2022). Tagged actin mRNA dysregulation in IGF2BP1<sup>-/-</sup> mice. Proc. Natl. Acad. Sci. USA 119, e2208465119.
- 86. Dolan, M.-J., Frechter, S., Bates, A.S., Dan, C., Huoviala, P., Roberts, R.J., Schlegel, P., Dhawan, S., Tabano, R., Dionne, H., et al. (2019). Neurogenetic dissection of the Drosophila lateral horn reveals major outputs, diverse behavioural functions, and interactions with the mushroom body. eLife 8, e43079.
- Aso, Y., Sitaraman, D., Ichinose, T., Kaun, K.R., Vogt, K., Belliart-Guérin, G., Plaçais, P.-Y., Robie, A.A., Yamagata, N., Schnaitmann, C., et al. (2014). Mushroom body output neurons encode valence and guide memory-based action selection in Drosophila. eLife 3, e04580.
- Bidaye, S.S., Laturney, M., Chang, A.K., Liu, Y., Bockemühl, T., Büschges, A., and Scott, K. (2020). Two brain pathways initiate distinct forward walking programs in Drosophila. Neuron 108, 469–485.e8.
- Kohwi, M., and Doe, C.Q. (2013). Temporal fate specification and neural progenitor competence during development. Nat. Rev. Neurosci. 14, 823–838.
- Sun, H., and Hobert, O. (2023). Temporal transitions in the postembryonic nervous system of the nematode *Caenorhabditis elegans*: recent insights and open questions. Semin. Cell Dev. Biol. 142, 67–80.
- 91. El-Danaf, R.N., Rajesh, R., and Desplan, C. (2023). Temporal regulation of neural diversity in Drosophila and vertebrates. Semin. Cell Dev. Biol. 142. 13–22.
- Al-Khindi, T., Sherman, M.B., Kodama, T., Gopal, P., Pan, Z., Kiraly, J.K., Zhang, H., Goff, L.A., du Lac, S., and Kolodkin, A.L. (2022). The transcription factor Tbx5 regulates direction-selective retinal ganglion cell development and image stabilization. Curr. Biol. 32, 4286–4298.e5.
- 93. Ahmed, M., Rajagopalan, A.E., Pan, Y., Li, Y., Williams, D.L., Pedersen, E.A., Thakral, M., Previero, A., Close, K.C., Christoforou, C.P., et al.

- (2023). Hacking brain development to test models of sensory coding. https://doi.org/10.1101/2023.01.25.525425.
- 94. Goldblatt, D., Huang, S., Greaney, M.R., Hamling, K.R., Voleti, V., Perez-Campos, C., Patel, K.B., Li, W., Hillman, E.M.C., Bagnall, M.W., et al. (2023). Neuronal birthdate reveals topography in a vestibular brainstem circuit for gaze stabilization. Curr. Biol. *33*, 1265–1281.e7.
- Stone, T., Webb, B., Adden, A., Weddig, N.B., Honkanen, A., Templin, R., Wcislo, W., Scimeca, L., Warrant, E., and Heinze, S. (2017). An anatomically constrained model for path integration in the bee brain. Curr. Biol. 27, 3069–3085.e11.
- Yilmaz, A., Gagnon, Y., Byrne, M., Baird, E., and Dacke, M. (2022). Coldinduced anesthesia impairs path integration memory in dung beetles. Curr. Biol. 32, 438–444.e3.
- Pisokas, I., Rössler, W., Webb, B., Zeil, J., and Narendra, A. (2022).
   Anesthesia disrupts distance, but not direction, of path integration memory. Curr. Biol. 32, 445–452.e4.
- Beetz, M.J., Kraus, C., Franzke, M., Dreyer, D., Strube-Bloss, M.F., Rössler, W., Warrant, E.J., Merlin, C., and el Jundi, B. (2022). Flightinduced compass representation in the monarch butterfly heading network. Curr. Biol. 32, 338–349.e5.
- el Jundi, B., Baird, E., Byrne, M.J., and Dacke, M. (2019). The brain behind straight-line orientation in dung beetles. J. Exp. Biol. 222, jeb192450.
- Lin, Y., Zhang, X.-J., Yang, J., Li, S., Li, L., Lv, X., Ma, J., and Shi, S.-H. (2023). Developmental neuronal origin regulates neocortical map formation. Cell Rep. 42, 112170.
- Gao, P., Sultan, K.T., Zhang, X.-J., and Shi, S.-H. (2013). Lineage-dependent circuit assembly in the neocortex. Development 140, 2645–2655.
- 102. Wang, Y.W., Wreden, C.C., Levy, M., Meng, J.L., Marshall, Z.D., MacLean, J., and Heckscher, E. (2022). Sequential addition of neuronal stem cell temporal cohorts generates a feed-forward circuit in the Drosophila larval nerve cord. eLife 11, e79276.
- 103. Liu, Z., Yang, C.-P., Sugino, K., Fu, C.-C., Liu, L.-Y., Yao, X., Lee, L.P., and Lee, T. (2015). Opposing intrinsic temporal gradients guide neural stem cell production of varied neuronal fates. Science 350, 317–320.
- 104. Marchetti, G., and Tavosanis, G. (2017). Steroid hormone ecdysone signaling specifies mushroom body neuron sequential fate via Chinmo. Curr. Biol. 27, 3017–3024.e4.
- 105. Rossi, A.M., and Desplan, C. (2020). Extrinsic activin signaling cooperates with an intrinsic temporal program to increase mushroom body neuronal diversity. eLife 9, e58880.
- 106. Guan, W., Bellemin, S., Bouchet, M., Venkatasubramanian, L., Guillermin, C., Laurençon, A., Kabir, C., Darnas, A., Godin, C., Urdy, S., et al. (2022). Post-transcriptional regulation of transcription factor codes in immature neurons drives neuronal diversity. Cell Rep. 39, 110992.
- 107. Samuels, T.J., Järvelin, A.I., Ish-Horowicz, D., and Davis, I. (2020). Imp/ IGF2BP levels modulate individual neural stem cell growth and division through myc mRNA stability. eLife 9, e51529.
- 108. Vijayakumar, J., Perrois, C., Heim, M., Bousset, L., Alberti, S., and Besse, F. (2019). The prion-like domain of Drosophila Imp promotes axonal transport of RNP granules in vivo. Nat. Commun. 10, 2593.
- Pfeiffer, B.D., Ngo, T.-T.B., Hibbard, K.L., Murphy, C., Jenett, A., Truman, J.W., and Rubin, G.M. (2010). Refinement of tools for targeted gene expression in Drosophila. Genetics 186, 735–755.
- Dionne, H., Hibbard, K.L., Cavallaro, A., Kao, J.-C., and Rubin, G.M. (2018). Genetic reagents for making Split-GAL4 lines in Drosophila. Genetics 209, 31–35.
- 111. Green, J., Vijayan, V., Mussells Pires, P., Adachi, A., and Maimon, G. (2019). A neural heading estimate is compared with an internal goal to guide oriented navigation. Nat. Neurosci. 22, 1460–1468.



#### **STAR**\***METHODS**

#### **KEY RESOURCES TABLE**

REAGENT or RESOURCE	SOURCE	IDENTIFIER
Antibodies		
Chicken anti-GFP Antibody, Polyclonal	Aves Lab	Cat#GFP-1010; RRID:AB_2307313
Mouse anti-Brp (nc82) Antibody, Monoclonal	DSHB	Cat#AB_2314866; RRID:AB_2314866
Rabbit anti-DsRed Antibody, Polyclonal	TaKaRa	Cat#632496; RRID:AB_10013483
Rabbit anti-Tachykinin Antibody	Jan Veenstra Lab	N/A
Rabbit anti-sNPF Antibody	Jan Veenstra Lab	N/A
Donkey Anti-Chicken IgY Antibody (Alexa Fluor 488)	Jackson ImmunoResearch	Cat#703-545-155; RRID:AB_2340375
Donkey Anti-Mouse IgG Antibody (Alexa Fluor 647)	Jackson ImmunoResearch	Cat#715-605-151; RRID:AB_2340863
Goat Anti-Rabbit IgG (H+L) Antibody (Alexa Fluor 555)	Invitrogen	Cat#A-21429; RRID:AB_2535850
Normal Donkey Serum	Jackson ImmunoResearch	Cat#017-000-121; RRID:AB_2337258
Normal Goat Serum	Jackson ImmunoResearch	Cat#005-000-121; RRID:AB_2336990
Chemicals, peptides, and recombinant proteins		
Schneider's Insect medium	Sigma-Aldrich	Cat#S0146
16% Paraformaldehyde (PFA)	Electron Microscopy Sciences	Cat#15710
TritonX-100	Sigma-Aldrich	Cat#T8787
DPX mounting medium	Sigma-Aldrich	Cat#06522
Deposited data		
Raw and analyzed data	This study	https://osf.io/nsrf8/
Experimental models: Organisms/strains		
VT029515-LexA	Nagel Lab	N/A
R21D07-LexA	BDSC	RRID:BDSC_ 54637
R12D12-LexA	BDSC	RRID:BDSC_ 52446
VT062617-LexA	Nagel Lab	N/A
15E12-GAL4	BDSC	RRID:BDSC_ 48608
65C03-GAL4	BDSC	RRID:BDSC_41290
VT029515-GAL4	VDRC	N/A
17A12-GAL4	BDSC	RRID:BDSC_45815
w [1118]; P{y[+t7.7] w[+mC]=R9D11- CD4-tdTom}attP2/TM6B, Tb[1]	BDSC	RRID:BDSC_35847
VT062617-GAL4	VDRC	N/A
Pointed-GAL4 (Chromosome 3)	Yuh-Nung Jan	N/A
LexAopmCD8GFP (Chromosome 3)	BDSC	RRID:BDSC_ 32207
Wor-GAL4, Ase-GAL80 (Chromosome 2)	Chris Doe Lab	N/A
		(Continued on next page

(Continued on next page)





Continued		
REAGENT or RESOURCE	SOURCE	IDENTIFIER
UAS-FLP-PEST (Chromosome X)	BDSC	RRID:BDSC_ 55807
UAS-FLP-D5 (Chromosome 2)	Rubin Lab, JRC	N/A
mCherry RNAi (Chromosome 3)	BDSC	RRID:BDSC_ 35785
LexAop-FRT-STOP-FRT-GFP (Chromosome 3)	BDSC	RRID:BDSC_ 57588
UAS-FLP-PEST; Wor-GAL4, Ase-GAL80; LexAop-FRT-stop-FRT-GFP	Syed Lab	N/A
dpn>KDRT-stop-KDRT>Cre:PEST; actin^LoxP-GAL80-stop-LoxP^LexA::P65, LexAop-rCD2::RFP-p10-spacer-UAS- mCD8::GFP-p10; stg14-KD	Tzumin Lee Lab	N/A
Hs-ATG>KOT>FLP, dpn>FRT-stop-FRT>Cre:PEST; actin^LoxP-GAL80-stopLoxP^LexA::P65, LexAop-rCD2::RFP-p10-spacer-UAS-mCD8::GFP- p10; stg14-KD	Tzumin Lee Lab	N/A
VT029515-LexA; Pointed-GAL4, LexAopGFP	This study	N/A
30E10-LexA; Pointed-GAL4, LexAopGFP	This study	N/A
65C03-LexA; Pointed-GAL4, LexAopGFP	This study	N/A
21D07-LexA, LexAopmCherryHA; Pointed-GAL4	This study	N/A
VT062617-LexA; Pointed-GAL4, LexAopGFP	This study	N/A
UAS-ImpRNAi; UAS-ImpRNAi (Chromosome 2 and 3)	Syed Lab	RRID:BDSC_38219 and RRID:BDSC_34977
Pin/CyO; UAS-Imp	Tzumin Lee Lab	N/A
W <sup>1118</sup>	BDSC	5905
UAS-ImpRNAi (Chromosome 3)	BDSC	RRID:BDSC_34977
UAS-SyncripRNAi	BDSC	RRID:BDSC_56972
Software and Algorithms		
lmajeJ	Open source	2.9.0/1.53t
Adobe Illustrator	Adobe Systems	(v27.2)
Adobe Photoshop	Adobe Systems	(v24.1.1)
Prism 9	GraphPad	(v9.5.1)
Zotero	Open source	(v6.0.26)
NI LabVIEW	National Instruments	Version 17.0
MATLAB 2021b	MATLAB	9.11.0.1769968 (R2021b)

#### **RESOURCE AVAILABILITY**

#### **Lead contact**

Further information and requests for resources and reagents should be directed to and will be fulfilled by the lead contact, Mubarak Hussain Syed (flyguy@unm.edu).

#### **Materials availability**

This study did not generate new unique reagents. Requests of fly stocks should be directed to and will be fulfilled by the lead contact, Mubarak Hussain Syed (flyguy@unm.edu).

#### **Data and code availability**

All data generated in this study has been made publicly available at https://osf.io/nsrf8/. This paper does not report original code.



Any additional information required to reanalyze the data reported in this work paper is available from the lead contact upon request.

#### **EXPERIMENTAL MODEL AND STUDY PARTICIPANT DETAILS**

For all experiments, we used *Drosophila melanogaster*. All the fly stocks were maintained at 25°C on standard cornmeal-agar medium and a 12h light-dark cycle. The RNAi and overexpression experimental crosses were raised at 29°C. Adult flies dissected were 3-7 days old. For behavioral experiments, female flies were collected at least 1 day after eclosion and then placed in vials that were situated in custom-made cardboard boxes at room temperature, with a 12-hour light-dark cycle, for at least two days to acclimate to ambient temperature and ensure correct circadian rhythm for the experimental time of day. All experiments were conducted within 4 hours after the flies' apparent "dawn" (ZT0-ZT4). The flies were then starved for 24 hr in an empty transparent polystyrene vial that contained a Kimwipe that was soaked in distilled water to humidify the air. By the day of the behavioral experiments, the flies had an average age of 3 to 7 days. Flies were anesthetized over ice for approximately 1 minute before being loaded into wind tunnels and allowed at least 5 minutes to recover before starting the first trial. The exact genotypes for each figure panel are listed in the table below. Parental strains and RRIDs are listed in the key resources table.

#### **METHOD DETAILS**

#### **Immunostaining**

Adult fly brains were dissected in Schneider's Insect medium (Sigma-Aldrich), and then fixed at room temperature for 23 min in 4% paraformaldehyde (EMS) in PBT buffer. 10X PBS buffer stock contained NaCl: 1.37 M, KCl: 27 mM, Na<sub>2</sub>HPO<sub>4</sub>: 100 mM, KH<sub>2</sub>PO<sub>4</sub>: 18 mM with a pH of 7.4. Working 1X PBT had an addition of 0.5% TritonX-100 (Sigma-Aldrich). Fixing was followed by washing at room temperature in PBT to remove PFA. The samples were blocked at room temperature for 40 min in PBT containing 2.5% normal goat serum (Jackson ImmunoResearch) and 2.5% normal donkey serum (Jackson ImmunoResearch). Adult brains were then incubated for 48hr at 4°C in the primary antibody solution. Primary antibody staining was followed by washing in PBS-T and then the adult brains were incubated for 2hr at room temperature in the secondary antibody solution. The brains were then washed in PBT. The primary and secondary antibody solutions were prepared in the blocking solution (prep described above).

Following the antibody staining, brains were mounted on the Poly-lysine-coated cover slips, serially dehydrated in alcohol with concentrations 30%, 50%, 75%, 95% and 3 rounds of 100% to replace PBT. The brains were then cleared in Xylene with 3 rounds of 5 min each and then mounted in DPX mounting medium, dibutyl phthalate in xylene (Sigma-Aldrich #06522). The samples were allowed to set in DPX for 3 days before imaging.

#### **Microscopy**

Images were acquired using a Zeiss LSM780 and LSM980 confocal microscope, analyzed using ImageJ, and processed using ImageJ and Photoshop. Cell body numbers were calculated manually using a cell counter in ImageJ, and the statistical analysis and graphs were made using GraphPad Prism. Two-tailed student t-tests were used to compare control with loss of function and gain of function respectively for cell body numbers. Asterisks denote levels of significant differences \*p<0.05; \*\*p<0.01; \*\*\*p<0.001.

#### **Birth-dating using Cell class lineage intersection system**

Males from neuron class specific GAL4 lines were mated to females from the CLIn line.<sup>81</sup> Egg collection was done for 3 to 4 hr intervals on apple juice containing agar plates. Hatched larvae (0-3 hr old) were manually collected and raised in standard fly food at 25°C. Heat shock was applied to the hatched larvae for 12-15 min for lineage analysis and 40 min for birth-dating at the time point 0 hr, 24 hr, 48 hr and 72 hr ALH. F1 adult flies of age 3-7 days were dissected.

#### **Behavioral Apparatus**

All behavioral experiments were performed in miniature wind tunnels. <sup>42</sup> Flies were constrained to walk in a shallow acrylic arena with a constant laminar wind at 10 cm/second. The wind tunnels were backlit using IR LEDS (850 nm, Environmental Lights) and movement was recorded using a camera placed below the chamber (Basler acA1920-155um). A 10 s pulse of odor (either 1% or 10% apple cider vinegar) was presented through Lee valves connected to the wind tunnel with polyethylene tubing. Within each 70 s trial, flies experienced 30 s of clean wind, 10 s of odor with wind, and then 30 s of clean wind again. All stimuli were controlled through a NIDAQ board. There are roughly 5 seconds between the end of one trial and the start of the next. Position (x,y) and orientation data were computed and collected in real time using a double-thresholding algorithm as described previously using NI LabVIEW).

#### **QUANTIFICATION AND STATISTICAL ANALYSIS**

#### **Analysis of Behavioral Data**

All analysis was completed using MATLAB (Mathworks, Natick, MA). Calculation of trajectory and basic movement parameters seen in Figure 6. A-C (ground speed, orientation, etc.) were completed using analysis code described in Álvarez-Salvado et al. 42





#### **Orientation histograms**

To compute orientation histograms, we pooled trials across all flies, and separated orientation data from the period before odor presentation, the period during the 10 seconds of odor, and the period following odor offset. We binned orientation data from the first 5 seconds of each of these periods into 36 bins of width 10 degrees. Error bars were created using jackknife resampling across flies and represent standard error calculated as:

$$SE = \frac{\sigma}{\sqrt{n}}$$

where  $\sigma$  is standard deviation and n is the number of samples. The resultant data, in polar coordinates, was then converted to Cartesian coordinates for ease of plotting and creation of error bars.

#### Histograms of ground speed and angular velocity

To compute groundspeed and angular velocity histograms, we again pooled data across flies. We binned values of ground speed and angular velocity into bins of width 1mm/s and 50 deg/s respectively (Figures 6E, 6F, 6H, and 6I) Histograms of both parameters were normalized to probability. Error bars represent standard error and were created using jackknife resampling with bias correction across all flies. Angular velocity of stationary flies (ground speed< 1mm/s) were excluded from analysis.

#### Summary plots of change in forward velocity and ground speed

Iterating through all trials for a single fly, we calculated the difference between the mean upwind velocity in the first 5 seconds of odor presentation and the mean upwind velocity in the 5 seconds preceding odor presentation. We then calculated the mean change in upwind velocity between these two periods for a single fly by averaging across all trials. For data representation, we then calculated the mean value across all flies, as well as the standard error. Significance was calculated using the mean value of each fly as a data point in an unpaired t test with Bonferroni correction for multiple comparisons using the equations:

$$t = \frac{\overline{x_1} - \overline{x_2}}{s_p \sqrt{\frac{1}{n_1} + \frac{1}{n_2}}}, s_p = \sqrt{\frac{(n_1 - 1)s_1^2 + (n_2 - 1)s_2^2}{n_1 + n_2 - 2}}$$

where  $\overline{x_1}$  and  $\overline{x_2}$  are sample means,  $n_1$  and  $n_2$  are sample sizes,  $s_\rho$  is the population variance, and  $s_1$  and  $s_2$  are the sample variances. The same logic was used for calculating change in ground speed and performing statistical testing (Figure 6J). Significance is marked with asterisks in the figure and the associated p-values can be found below.

#### **Upwind Velocity**

Comparison	p-Value
Pointed-GAL4>UAS-mCherryRNAi compared to Pointed-GAL4>UAS-ImpRNAi;ImpRNAi	p = 5.906x10^-11
Pointed-GAL4>UAS-mCherryRNAi compared to Pointed-GAL4>UAS-ImpRNAi (III)	p = 1.1476x10^-9
Pointed-GAL4>UAS-mCherryRNAi (1:10) compared to Pointed-GAL4>ImpRNAi;ImpRNAi (1:10)	p = 1.2293x10^-4
Pointed-GAL4>UAS-mCherryRNAi (1:10) compared to Pointed-GAL4>UAS- SypRNAi(1:10)	p = 0.0042
DL1-GAL4>UAS-mCherryRNAi compared to DL1-GAL4>UAS- ImpRNAi;ImpRNAi	p = 9.922x10^-6

#### **Ground Speed**

Comparison	p-Value
Pointed-GAL4>UAS-mCherryRNAi compared to Pointed-GAL4>UAS-ImpRNAi (III)	p= 0.0015
Pointed-GAL4>UAS-mCherryRNAi compared to Pointed-GAL4>UAS-Imp	p= 7.7113x10^-4
DL1-GAL4>UAS-mCherryRNAi compared to DL1-GAL4>UAS- ImpRNAi;ImpRNAi	p = 2.2281x10^-7



Fly cross	Figure Panel
UAS-FLP-PEST; Wor-GAL4, Ase-GAL80; LexAop-FRT-stop-FRT-GFP crossed to VT029515-LexA	Figure 2C
UAS-FLP-PEST; Wor-GAL4, Ase-GAL80; LexAop-FRT-stop-FRT-GFP crossed to VT062617-LexA	Figure 2D
UAS-FLP-PEST; Wor-GAL4, Ase-GAL80; LexAop-FRT-stop-FRT-GFP crossed to R21D07-LexA	Figure 2E
UAS-FLP-PEST; Wor-GAL4, Ase-GAL80; LexAop-FRT-stop-FRT-GFP crossed to R12D12-LexA	Figure 2F
dpn>KDRT-stop-KDRT>Cre:PEST; actin^LoxP-GAL80-stop-LoxP^LexA::P65, LexAop-rCD2::RFP-p10-spacer-UAS-mCD8::GFP-p10; stg14-KD crossed to 65C03-GAL4	Figure 2H
dpn>KDRT-stop-KDRT>Cre:PEST; actin^LoxP-GAL80-stop-LoxP^LexA::P65, LexAop-rCD2::RFP-p10-spacer-UAS-mCD8::GFP-p10; stg14-KD crossed to 15E12-GAL4	Figure 2I
Hs-ATG>KOT>FLP, dpn>FRT-stop-FRT>Cre:PEST; actin^LoxP-GAL80- stopLoxP^LexA::P65, LexAop-rCD2::RFP-p10-spacer-UAS-mCD8::GFP-p10; stg14-KD crossed to VT029515-GAL4	Figures 3D–3H
UAS-FLP; 17A12-GAL4 crossed to VT029515-LexA; LexAop-FRT-stop- FRT-GFP	Figure 3J
VT029515-LexA; Pointed -GAL4, LexAopGFP	Figures 4A-4A"
VT029515-LexA; Pointed -GAL4, LexAopGFP crossed to UAS-ImpRNAi; UAS-ImpRNAi	Figures 4B–4B"
VT029515-LexA; Pointed-GAL4, LexAopGFP crossed to Pin/CyO; UAS-Imp	Figures 4C-4C"
UAS-FLP; TK-GAL4 crossed to VT029515-LexA; LexAop-FRT-stop-FRT-GFP	Figures 4D-4D"
VT029515-LexA; 17A12-GAL4, LexAopGFP	Figure 4E
VT029515-LexA; 17A12-GAL4, LexAopGFP crossed to UAS-ImpRNAi; UAS-ImpRNAi	Figure 4E'
UAS-GFP; VT029515-GAL4	Figures 4F-4F"
UAS-GFP; VT029515-GAL4 crossed to UAS-ImpRNAi; UAS-ImpRNAi	Figures 4G–4G"
30E10-LexA; Pointed-GAL4, LexAopGFP	Figure 5A
30E10-LexA; Pointed-GAL4, LexAopGFP crossed to UAS-ImpRNAi; UAS-ImpRNAi	Figure 5B
30E10-LexA; Pointed -GAL4, LexAopGFP crossed to Pin/CyO; UAS-Imp	Figure 5C
65C03-LexA; Pointed-GAL4, LexAopGFP	Figure 5D
65C03-LexA; Pointed-GAL4, LexAopGFP crossed to UAS-ImpRNAi; UAS-ImpRNAi	Figure 5E
65C03-LexA; Pointed-GAL4, LexAopGFP crossed to Pin/CyO; UAS-Imp	Figure 5F
21D07-LexA, LexAopmCherryHA; Pointed -GAL4	Figure 5G
21D07-LexA, LexAopmCherryHA; Pointed GAL4 crossed to UAS-ImpRNAi; UAS-ImpRNAi	Figure 5H
21D07-LexA, LexAopmCherryHA; Pointed-GAL4 crossed to Pin/CyO; UAS-Imp	Figure 5I
VT062617-LexA; Pointed-GAL4, LexAopGFP	Figure 5J
VT062617-LexA; Pointed-GAL4, LexAopGFP crossed to UAS-ImpRNAi; UAS-ImpRNAi	Figure 5K
VT062617-LexA; Pointed -GAL4, LexAopGFP crossed to Pin/CyO; UAS-Imp	Figure 5L
VT029515-LexA; Pointed-GAL4, LexAopGFP	Figures 5Q-5U
VT029515-LexA; Pointed-GAL4, LexAopGFP crossed to UAS-ImpRNAi; UAS-ImpRNAi	Figures 5Q'–5U'
Pointed-GAL4/UAS-mCherryRNAi	Figures 6A and 6C-6F
UAS-ImpRNAi/+; Pointed-GAL4/UAS-ImpRNAi	Figures 6B and 6C-6F
17A12-GAL4/UAS-mCherryRNAi	Figures 6G–6I
UAS-ImpRNAi/+; 17A12-GAL4/UAS-ImpRNAi	Figures 6G–6I
	(Continued on next page





Continued		
Fly cross	Figure Panel	
Pointed-GAL4/UAS-ImpRNAi	Figure 6J	
Pointed-GAL4/w <sup>1118</sup>	Figure 6J	
Pointed-GAL4 UAS-SypRNAi	Figure 6J	
Pin/+;UAS-Imp/+; Pointed-GAL4/UAS-Imp	Figure 6J	
17A12-GAL4/UAS-mCherryRNAi	Figure 6J	
1UAS-ImpRNAi/+; 7A12-GAL4; UAS-ImpRNAi	Figure 6J	
17A12-GAL4/UAS-SypRNAi	Figure 6J	
Pin/+; 17A12-GAL4 /UAS-Imp	Figure 6J	